IEEE Access
Multidisciplinary | Rapid Review | Open Access Journal

Received April 30, 2020, accepted May 26, 2020, date of publication June 1, 2020, date of current version June 11, 2020.

Digital Object Identifier 10.1109/ACCESS.2020.2999053

A Survey on Antenna Designs for Breast Cancer Detection Using Microwave Imaging

HILAL M. EL MISILMANI[1], (Member, IEEE), TAREK NAOUS[1], (Student Member, IEEE), SALWA K. AL KHATIB[1], (Student Member, IEEE), AND KARIM Y. KABALAN[2], (Member, IEEE)

[1]Electrical and Computer Engineering Department, Beirut Arab University, Beirut 1107 2809, Lebanon
[2]Electrical and Computer Engineering Department, American University of Beirut, Beirut 1107 2020, Lebanon

Corresponding author: Hilal M. El Misilmani (hilal.elmisilmani@ieee.org)

ABSTRACT With the prevalence of breast cancer among women and the shortcomings of conventional techniques in detecting breast cancer at its early stages, microwave breast imaging has been an active area of research and has gained momentum over the past few years, mainly due to the advantages and improved detection rates it has to offer. To achieve this outcome, specifically designed antennas are needed to satisfy the needs of such systems where an antenna array is typically used. These antennas need to comply with several criteria to make them suitable for such applications, which most importantly include bandwidth, size, design complexity, and cost of manufacturing. Many works in the literature proposed antennas designed to meet these criteria, but no works have classified and evaluated these antennas for the use in microwave breast imaging. This paper presents a comprehensive study of the different array configurations proposed for microwave breast imaging, with a thorough investigation of the antenna elements proposed to be used with these systems, classified per antenna type, and per the improvements that concern the operational bandwidth, the size of the antenna, the radiation characteristics, and the techniques used to achieve the improvement. At the end of the investigation, a qualitative evaluation of the antenna designs is presented, providing a comparison between the investigated antennas, and determining whether a design is suitable or not to be used in antenna arrays for microwave breast imaging, based on the performance of each. An evaluation of the investigated arrays is also presented, where the advantages and limitations of each array configuration are discussed.

INDEX TERMS Antenna design, antenna arrays, breast cancer detection, microwave breast imaging, ultra wideband antennas (UWB).

I. INTRODUCTION

Breast cancer is the most common cancer among women in developed and developing countries and it is the leading cause of cancer-related deaths among women worldwide [1], [2]. When accounting for both sexes, breast cancer is the second most common cancer after lung cancer [3]. Cancer screening is a practice that reduces disease-specific morbidity and mortality since early detection has been shown to positively affect the outcome of the disease.

The first stage of breast cancer detection is the identification of an abnormality in the breast tissue with either physical examinations or imaging techniques such as mammography and ultrasound [5]. However, mammograms are not always accurate, as the rate of false negative mammograms has been reported between 1977 and 1998 to be ranging from 4% to 34% [6]. Such results, which are due to the inherent limitations of X-ray mammography, consequently lead to increasing disease-specific morbidity and mortality as diagnosis and treatment may be delayed due to the false sense of security given to affected women [6]. This imaging technique is often painful as it requires breast compression [7], and it exposes the patient to ionizing radiation [8]. Ionizing radiation is considered to be an associated risk with mammography [9]. It was also shown in [10], [11] that screening mammography gives less sensitive results for women with radiographically dense breast tissue.

Ultrasound imaging is frequently a follow-up to X-ray mammograms. It helps with the evaluation of lumps that are difficult to see on a mammogram, especially in dense

The associate editor coordinating the review of this manuscript and approving it for publication was Masood Ur-Rehman.

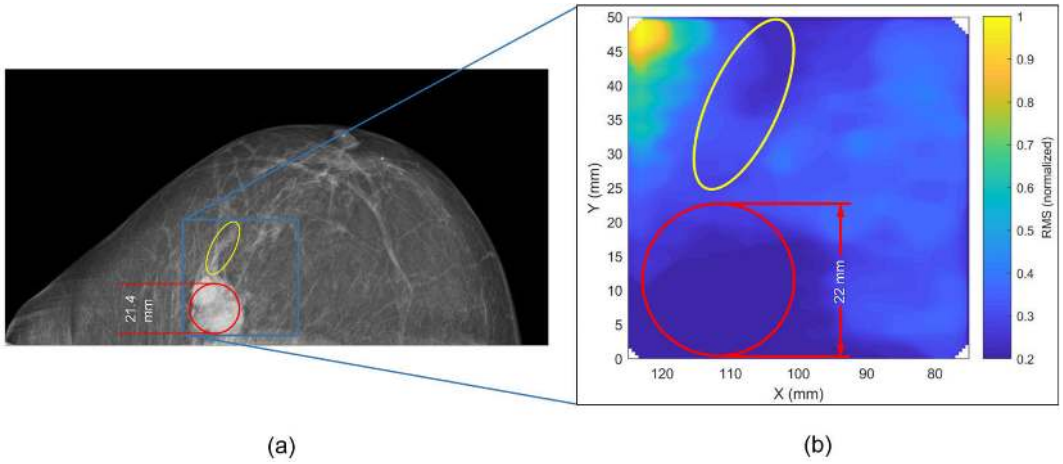

FIGURE 1. Comparison between X-ray image and microwave image for cancer patient. The lowest intensity values occur in the area of the tumor location given by stronger attenuation of cancerous tissue [4].

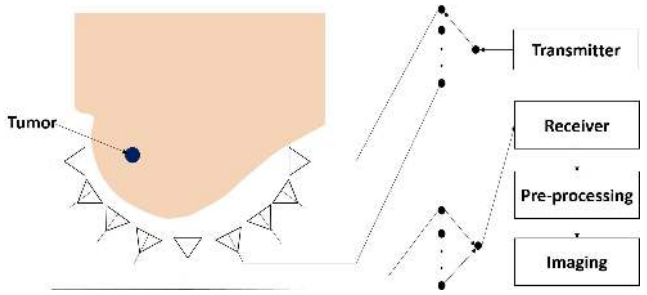

FIGURE 2. Typical microwave breast imaging system.

breasts. Similar to mammograms, ultrasound is a detection technique that has inherent limitations. Though it is a painless technique when compared to mammography, ultrasound falls short when distinguishing between malignant and benign tumors. It also has low resolution [12]. Thus, there exists a need to explore other detection techniques that are both efficient and accurate.

Microwave imaging [13] is developing as a promising technology with various biomedical applications. In the case of breast imaging, this technique entails transmitting short pulses of low-power microwaves into the breast tissue. Antennas positioned around the breast are used to collect the backscattered energy, and the received signals are used to produce a three-dimensional image of the scanned breast. Fig. 1 shows a comparison between an X-ray image and a microwave image for a cancer patient. The lowest intensity values, in Fig. 1b, indicate the location of the tumor as a result of the stronger attenuation caused by cancerous tissue.

A typical microwave breast imaging system is shown in Fig. 2. Multiple antennas operating in the near-field region are placed closely, in a specific array configuration, around the breast of a patient. Transmitting antennas are sequentially selected to illuminate the breast with microwave pulses. Reflections and backscattered signals are then collected by receiver antennas. The obtained data is then pre-processed and used for image reconstruction.

Many reasons are behind the wide appeal of this new detection technique; we present a selected few. Firstly, the conductivity σ and permittivity ϵ differ from normal human breast tissues and malignant human breast tissues over the range of microwave frequency [14], which can be used to detect the presence of tumors. Second, it produces a high-contrast three-dimensional image that is, in theory, equally effective for dense breast tissues [5]. Third, it does not require using ionizing radiation as in X-ray mammography, and breast compression is avoided [15]. Lastly, breast energy absorptions will be small due to the power levels adopted and repetition periods, which makes it unlikely for patients to suffer from potential health risks [16].

To this end, a plethora of antennas with design requirements tailored to this application have been proposed in the literature. Specific microwave antennas have been designed for transmitting and receiving short pulses where a scattering map could be created to spot the cancerous tumor. Many modifications and techniques have been introduced in the literature to improve the antenna's performance in terms of bandwidth, size, and radiation characteristics.

We start our survey by providing a brief overview on microwave breast imaging covering the different approaches adopted in the literature, along with the image reconstruction algorithms used. The desired antenna characteristics to satisfy the needs and challenges of such imaging systems are then discussed. Next, we classify the available antenna elements designs in the literature by type of enhancement that pertain to bandwidth, miniaturization, and/or radiation characteristics, and further by the antenna type and the technique used. These antennas include Vivaldi antennas, monopole antennas, bowtie antennas, in addition to fractal, and horn antennas. After investigating the antenna elements, the different antenna array configurations proposed in the literature to be used with microwave breast imaging systems are then investigated and classified as planar, enclosed, and hemispherical arrays. After investigating the proposed antenna

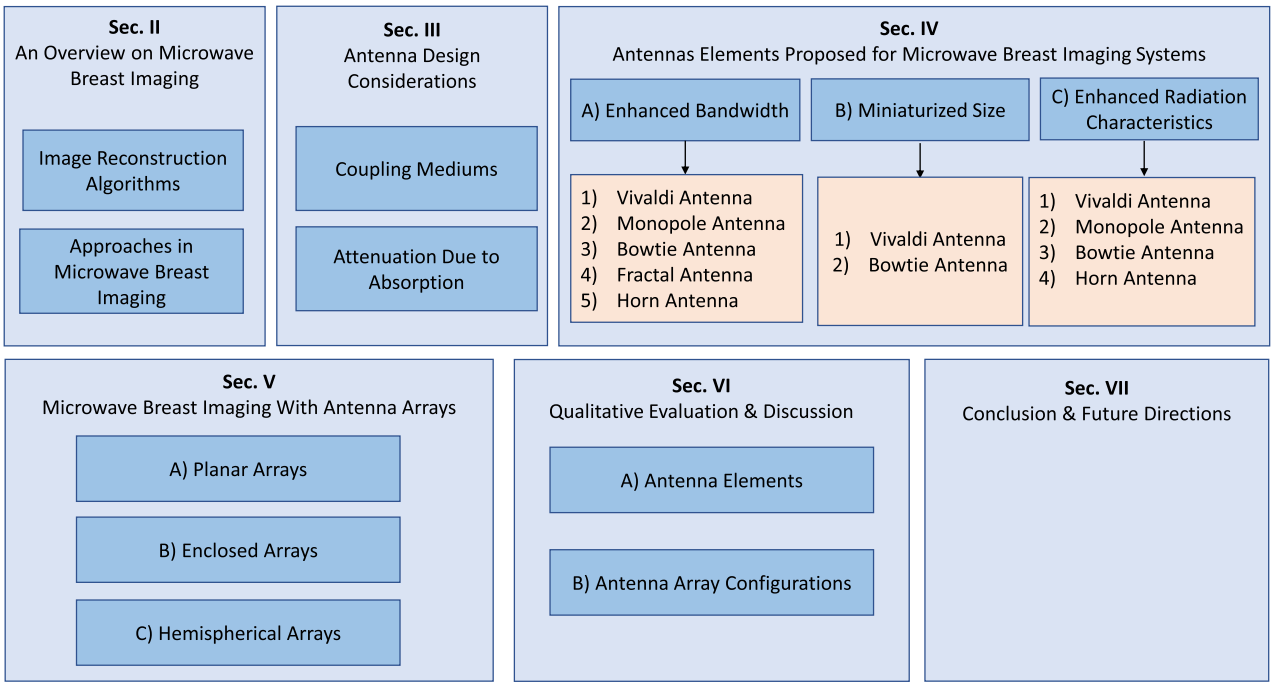

FIGURE 3. Diagrammatic view of the organization of this survey.

designs, a qualitative evaluation of the antennas discussed that will highlight the advantages and shortcomings of these antennas and determine which are more suitable to be used in antenna array systems for microwave breast imaging is presented. This is also followed by an evaluation of the different arrays presented in the literature for microwave breast imaging, which draws several conclusions about each type of array configuration. Tables that summarize the different investigated antennas and antenna arrays, and compare their performance, are also given. We note here that several surveys on microwave breast imaging exist in the literature [12], [17], [18], but none investigates the large number of antennas and antenna arrays provided here, with a thorough investigation of the different enhancements and techniques used to improve the design of each presented antenna.

The rest of this survey is organized as illustrated in Fig. 3, and as follows: Section II presents an overview on the different approaches in microwave breast imaging. In Section III, the challenges that face the design of these antennas related to coupling and absorption are provided. A thorough investigation of the antenna elements proposed in the literature for microwave breast imaging is then presented in Section IV, where the antennas are classified per improvement, the antenna type, and the technique used. The complete antenna system, as antenna arrays, are then presented in Section V classified per antenna array configuration. A qualitative evaluation of the different antenna elements and antenna array configurations is then presented in Section VI. Concluding remarks follow in Section VII.

II. AN OVERVIEW ON MICROWAVE BREAST IMAGING

Over the past few years, reconstruction algorithms for microwave imaging have witnessed an important attention. The interest in developing these near-field algorithms has been motivated by the failure of diffraction-limit approximations [19] as a foundation for image reconstruction, demanding the need for adequate algorithms where the full-wave electromagnetic interactions in tissues would be properly accounted for.

Previously, the imaging region took place in the far field, which required the use of antennas with increased directivity and gain while operating in the lower gigahertz frequency range ($1 - 3$ GHz). For this, waveguide antennas [20] were employed as the radiators. This has been eliminated with the introduction of near-field imaging, where different transmit antenna configurations are considered. For instance, a monopole antenna can be placed at the proximity of the breast while successfully illuminating the whole area, whereas the previously used waveguide antennas needed to be placed farther away from the breast area, in order for the main lobe of the antenna to provide adequate coverage. Additionally, a monopole has a much smaller and more flexible size, offering better economy-of-space than the waveguide antenna and making it a more attractive choice when considering an array design. Therefore, near-field imaging has surfaced as a promising approach for clinical settings.

Several approaches have been explored in the literature for breast imaging at microwave frequencies, which are active, passive, and hybrid approaches [21], shown in Fig. 4.

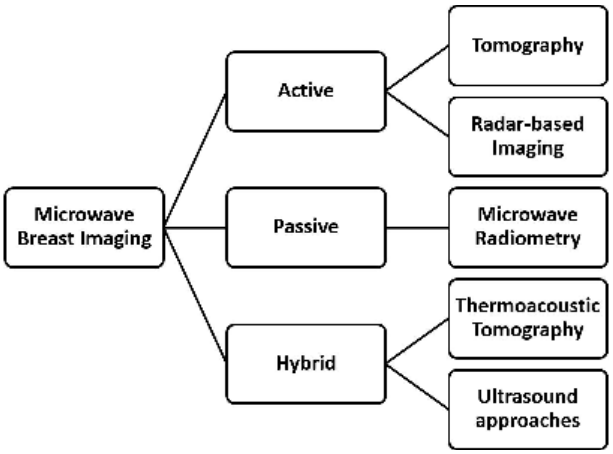

FIGURE 4. The different approaches and methods in microwave imaging.

In the active approach, the breast is illuminated with microwave radiation by the means of several antennas. Transmitted and reflected energy can then be collected and used to form images by using imaging algorithms. The presence of a tumor causes scattering of the incident waves due to the change in electrical properties. Using the information contained in the detected energies, microwave images can be constructed [22]. These algorithms perform coherent addition of backscattered radar signals, that are received after illumination of the breast with UWB pulses. They can be divided into two categories: data independent (DI) and data adaptive (DA) algorithms. DI algorithms perform the cohered addition based on an assumed propagation model, while in DA algorithms the propagation model is estimated from the received signals after compensation factors are applied to the channel model. Several algorithms have been proposed in literature and evaluated in [23], including: Delay-And-Sum (DAS) [24], Delay-Multiply-And-Sum (DMAS) [25], Improved Delay-And-Sum (IDAS) [26], Coherence Factor Based DAS (CF-DAS) [27], Channel Ranked DAS (CR-DAS) [28] and Robust Capon Beamformer (RCB) [29]. In this respect, there are two main approaches to create microwave images, which are transmission-reflection imaging and reflection imaging.

In the transmission-reflection imaging, known as microwave tomography [30]–[33], a single antenna is used to transmit microwave signals that travel through the breast and are then received by several receiver antennas at the opposite side of the breast, placed at equal distances from the surface of the breast. This process is repeated for several positions of the transmitting antenna. By using the incident and received fields, the shape of the breast and the spatial distribution of the permittivity can be obtained to create maps based on the electrical properties of the breast. An example showing a microwave tomographic permittivity image is shown in Fig. 5. Through signal processing the measured data is then used to create a map of the relative permittivity geometric distributions of the breast. Tumours usually reduce the strength of the scattered signal, hence any observed

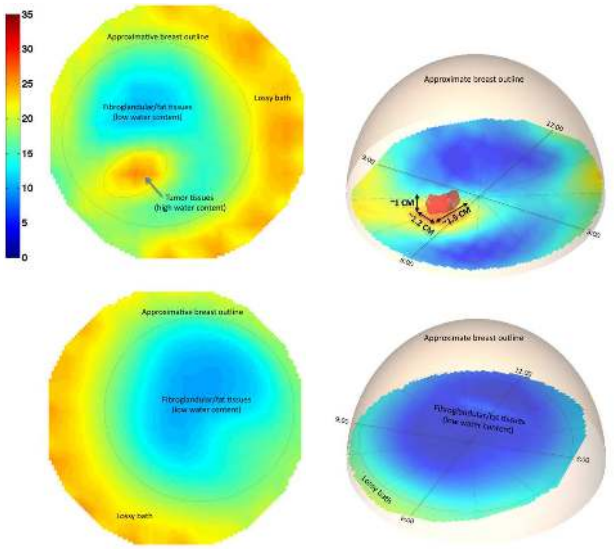

(a) (b)

FIGURE 5. Microwave tomographic permittivity images at 1300 MHz: upper, right breast; lower: left breast. (a) 2D images, (b) 3D images [34] (©[2012] IEEE).

areas of higher relative permittivity and conductivity values corresponds to the presence of tumour cells. Solving inverse scattering problems, the dielectric profile of the tissue under test is then deduced.

In reflection imaging, known as radar-based imaging or confocal microwave imaging (CMI) [24], [35]–[38], the reflections are summed or synthetically focused to create the images, using the time-delay from each antenna to a focal point. The reflected waves are the only ones used to form the images. The ideas adopted in this approach are mainly inspired by radio detection and ranging (Radar) systems. Basically, antennas are used to transmit microwave pulses or modulated harmonic microwave signals. Reflections are then received by the same transmitting antennas or by receiver antennas positioned in different locations. This approach can be used to localize tumors by using simpler algorithms that focus the reflected energy from the breast, thus providing a complete profile of the dielectric properties of the breast. An example showing cross-sectional images of radar-based imaging is shown in Fig. 6.

These two different approaches require different antenna characteristics. Microwave tomography is considered as a narrowband approach where antennas that operate in the lower frequency range ($1 - 6$ GHz) are needed, since high frequency signals will have limited penetration in the breast tissue, tumor, and skin. In radar-based imaging approach, the antennas require a wideband performance to achieve high resolution image reconstruction [40].

The passive approach, known as microwave radiometry, has been a research subject for many years [41]–[43]. It assumes that malicious tumors possess higher temperatures compared with healthy breast tissues. Based on this assumption, the difference in temperature between the normal and malignant tissues can be measured and used to draw conclusion.

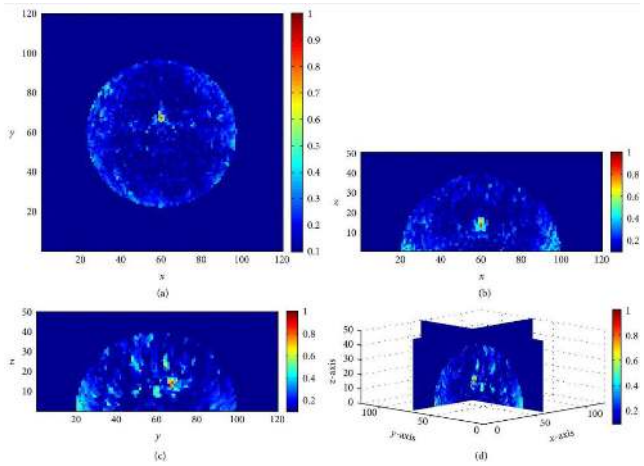

FIGURE 6. Cross-sectional images of restored breast model using radar-based imaging, (a) x-y plane, z = 17 mm, (b) x-z plane, y = 70 mm, (c) y-z plane, x = 60 mm, and (d) 3D image [39].

The hybrid approach is based on microwave-acoustic imaging where microwave signals are used to selectively heat tumors [44]. As a result of this heating, pressure-wave signals are generated which can be measured by ultrasound transducers. This collected data can then be useful in image construction.

III. ANTENNA DESIGN CONSIDERATIONS

Ever since microwaves caught the interest of engineers developing biomedical imaging devices, there has been a huge focus on finding suitable antennas that can satisfy the needs of such imaging systems. By transmitting short pulses into the breast area and based on the dielectric contrast between malicious and healthy breast tissues, the differentiated scattering can be obtained and used to construct images and localize tumors.

The design of the antenna is critical to the overall microwave imaging system performance. For microwave breast imaging systems, which are mainly an array of antennas, the antenna element needs to exhibit a broadband behavior, by being capable of radiating pulses over a wide range of frequencies with high fidelity, while maintaining a fair value of the gain. This has turned the attention to the usage of antennas operating in the Ultra-Wideband (UWB) that have been allocated a 7.5 GHz bandwidth (3.1 to 10.6 GHz) by the Federal Communication Commission (FCC) for UWB measurements, communications, and radar [45].

Also, the antenna needs to have a compact size so that it would occupy a small area on the total surface area of the breast. Complexity and cost of the design are also important factors that needs to be considered. Ideal breast imaging tools are labeled as cost effective and widely available, the fact which demands the suitable antenna to be easy and cheap to fabricate. A complex design might also be disadvantageous for some image reconstruction algorithms that can find it impractical to model the antenna.

As the antennas proposed for microwave imaging are designed to be used in the near-field, as discussed in Section II, this imposes several challenges on the design of the antennas. In addition to the rapid decrease of the fields with distance, and its effect on the absorption, several challenges arise that need to be considered in the design of suitable antennas for this application. For instance, as a result of working in the near-field, the antennas need to be placed very close to the breast, which could result in reflections that occur in the air-skin interface. Another challenge is found in the properties of the breast tissues that could result in the attenuation of the field reflected to the antennas. The rest of this section investigates these two challenges on the design of antennas for microwave imaging.

A. COUPLING MEDIUM

One of the challenges that needs to be taken into consideration in the design of antennas is the reflections that occur in the air-skin interface that can have magnitudes higher than the reflected tumor response. This issue can be alleviated by immersing the antenna in a coupling medium that possess dielectric characteristics similar to those of breast tissues. This problem is mainly seen in the enclosed arrays as will be discussed in Section V.

The coupling medium in its turn has its own effect on the antenna performance and radiation characteristics. Since the coupling medium will have a specific conductivity value, the propagation constant k will change in value taking into account the permittivity of the coupling medium. The modified propagation constant can be written as in (1) [46], with $\epsilon_r = \epsilon_r' - j\epsilon_r''$ being the permittivity of the coupling medium. If the coupling medium has no losses, ϵ_r'' will be zero.

$$k' = \omega\sqrt{\mu_0\epsilon_0(\epsilon_r' - j\epsilon_r'')} \tag{1}$$

This variation in the propagation constant inside the coupling medium changes the value of the wavelength. This will alter the current distribution of the antenna in the coupling medium, and hence will affect its input impedance and radiation characteristics. In addition, a lossy coupling medium will also introduce additional loss to the decay factor between source and the observation point. For this, the design of antennas should take into account the input impedance of the immersion coupling medium to properly match the antenna, and avoid degrading the performance of the imaging system. In addition, an understanding of the behavior of the proposed antenna in different conductivity materials of different electric properties is important to predict the performance of the antenna in the coupling medium.

B. ATTENUATION DUE TO ABSORPTION

Another challenge in the design of antennas for microwave imaging is the attenuation due to the absorption by the breast tissues. Microwave breast imaging systems are greatly influenced by the shape, size, and content tissues distribution of the breast. The breast is an in-homogeneous organ that undergoes anatomical transformation as a woman reaches

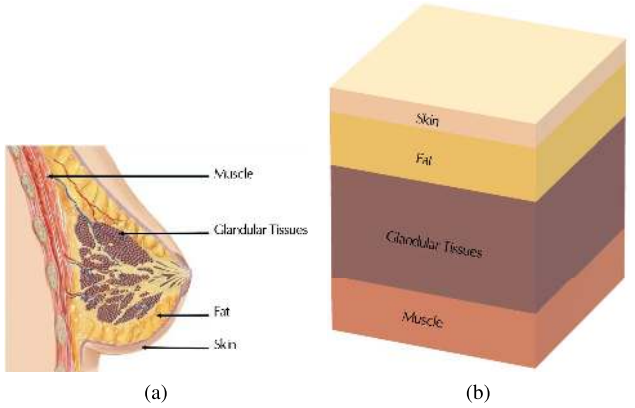

FIGURE 7. Simplified breast model (a) female breast structure, (b) stacked layers of the breast [47].

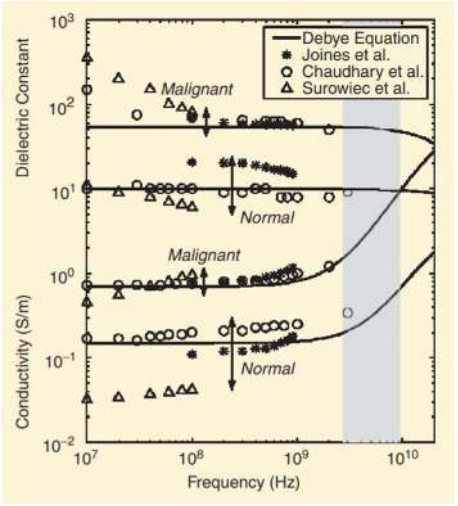

FIGURE 8. Single-Pole Debye curve fits of data samples for dielectric properties of normal and malignant breast tissues at radio and microwave frequencies [56] (©[2001] IEEE).

puberty until menopause and beyond. Having a protruding conical form with a circular base, a mature breast is composed of several underlying tissues. Lobes made of smaller lobules of glandular tissues, where cancer tumors usually originate, emanate from the nipple. These lobes are surrounded by the adipose layer, which are the fatty tissues extended throughout the breast, giving it its shape and size. The adipose layer is finally topped by the skin layer as shown in the simplified sketch of Fig. 7.

An important aspect to consider in designing microwave imaging systems is the several parameters that affect the transmission and reception of the microwave signals through these tissues. Taking into account the electric properties of the breast tissues, the design of the antenna has to consider the propagation and penetration loss due to the biological tissues. These tissues have varying conductivity and dielectric constants that depend on the type of the biological tissue (muscle, glandular tissues, fat, or skin), and the frequency of operation, leading to complex simulation and testing procedures. When breast tissues are exposed to microwaves, the Specific Absorption Rate (SAR), measured in W/kg, is used to obtain the power absorbed in a volume of the tissues [22]. The SAR can be obtained by averaging over a 1g of tissue in the shape of a cube, using (2), where dW is the incremental energy, dV is the volume element and ρ is the density of the volume. As per the Safety Standards [48], [49], the SAR threshold level is taken to be 1.6 W/kg, and 2 W/kg in Europe.

$$SAR = \frac{dW}{\rho dV} \tag{2}$$

In experimental microwave imaging research, testing must take place on breast phantoms to obtain more realistic results. These phantoms can be obtained by creating several mixtures that are Oil-in-Gelatin-Based [50], Triton X-100-Based [51], or other materials [27], [52].

In order to account for the differences in the electric properties of free-space and those of the breast tissues, the phantoms are required to mimic the breast tissue electric properties. These properties have been a subject of research for many years [14], [53]–[55], and they include the relative permittivity ϵ_r and the conductivity σ. Tissues with a higher water content have a higher permittivity and conductivity than tissues with low water content. It has been shown that, at microwave frequencies, changes also occur to these properties with the variation in frequency. As microwaves travel through tissues with a higher water content such as skin or tumors, more attenuation occurs compared to tissues with lower water content due to the absorbed energy.

Most of the work done on finding the dielectric constants of the different body tissues and organs are based on the relaxation model, known as the Cole-Cole equation, which reduces to Debye model, well known in measuring the dielectric properties of normal and malignant breast tissues [56]. Based on Debye model, Fig. 8, shows the dielectric properties of normal and malignant breast tissues at radio and microwave frequencies. In addition, Fig. 9 illustrates these changes on oil, fat, skin, and tumor tissues from 0 to 7 GHz and shows that malignant tissues have higher dielectric properties than healthy tissues [57].

IV. ANTENNA ELEMENTS PROPOSED FOR MICROWAVE BREAST IMAGING SYSTEMS

In this section, the different antennas proposed in the literature to be used as antenna elements for microwave breast imaging systems are investigated. These antennas mainly include Vivaldi antennas, monopole antennas, bowtie antennas, and fractal antennas, in addition to horn antennas. As the aim in antenna design works is to optimize antennas for a specific application and desired characteristics, the investigated antennas in this section are classified as per the enhancement done in each, including: enhanced bandwidth, miniaturized size, and enhanced radiation characteristics. In each of these classes, the antennas are further grouped based on their type, and then based on the technique used in each to achieve this enhancement.

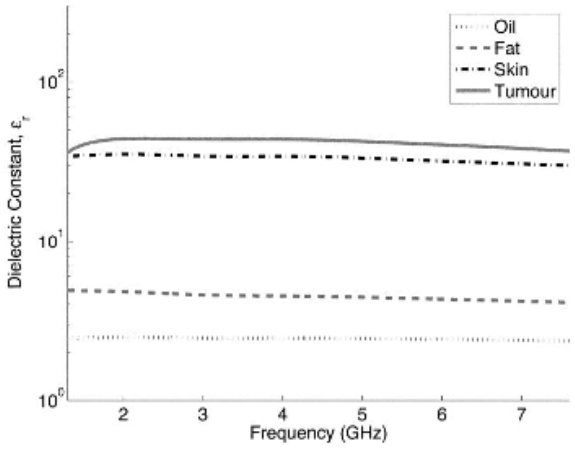

(a)

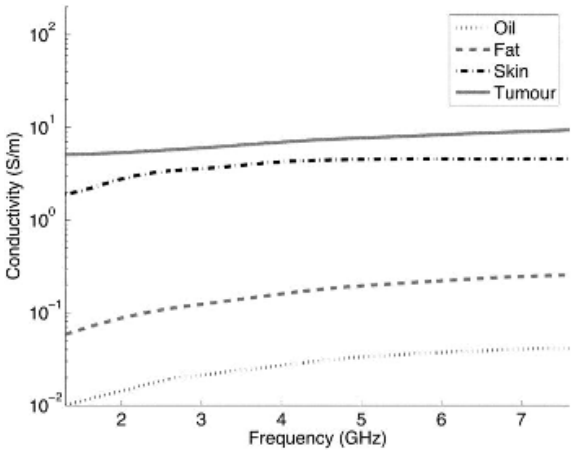

(b)

FIGURE 9. Variations of the (a) Relative Permittivity and (b) Conductivity of Oil, Fat, Skin, and Tumor Tissues with the Change in Frequency over the Range of 0 – 7 GHz [57] (©[2005] IEEE).

A. ENHANCED BANDWIDTH

1) VIVALDI ANTENNA

Due to their broadband behavior, Vivaldi antennas (VA), also known as exponentially tapered slot antennas, have been also the subject of interest for several years [58], [59].

a: CORRUGATIONS

Adding corrugations to the conventional Vivaldi structure can help achieve a broader bandwidth and higher gain. A Vivaldi antenna with improved corrugated edges was presented in [60] that has an operational bandwidth of $1 - 3$ GHz and a return loss of less than -10 dB. This structure showed an improved radiation pattern as a result of the corrugations introduced at the edges of the Vivaldi substrate. The improvement in the radiation pattern was achieved by using two corrugation lengths, 16 mm and 15 mm, with a constant corrugation width of 1.2 mm. In [61], the lengths of the corrugations in a Vivaldi antenna were independently optimized to reach a broader input impedance bandwidth than in [60] of $1.96 - 8.61$ GHz. The distance L_f between the first slot and the feed of the Vivaldi antenna, the distance W_gap between each slot, and the width W_s of each slot were also optimized to 20.2 mm, 1.07 mm, and 1.13 mm, respectively. It was shown that increasing the number of corrugations and varying their lengths between $5 - 25$ mm resulted in a wider bandwidth and higher gain when compared with a generic Vivaldi of the same size. Furthermore, corrugation at the flares and grating elements in the area of tapered slot were used in a Vivaldi antenna in [62], where an even wider impedance bandwidth from 2.9 GHz to more than 12 GHz was measured. The radiating structure of the Vivaldi antenna has a circular cavity on one end of the exponential tapered slot, which acts as an open circuit that minimizes the reflections from microstrip line. As a result, the proposed antennas showed a stable unidirectional radiation in E-plane and H-plane.

b: BALANCED ANTIPODAL VIVALDI ANTENNA

Another modification to the conventional Vivaldi antenna structure is found in [63] that presented a balanced antipodal Vivaldi antenna (BAVA). The BAVA is composed of three copper layers. The central layer acts as the conductor, while the external layers are considered as the ground plane. Substrate layers are placed on the sides of the antenna, and between the three copper layers as a separation. This geometry of the antenna helps balancing the dielectric load between the ground planes and the conductor. A narrower beamwidth of the antenna was obtained by introducing a director element in the antenna's structure resulting in a BAVA with Dielectric Director (BAVA-D). This improved directivity allowed for having more back-scattered energy from the breast which translates into better quality imaging. Both antennas are capable of operating over a broad frequency range of 2.4 to 18 GHz. Nevertheless, it was shown in [64], based on experiments, that BAVA-D antennas outperform BAVA antennas in tumor response localization.

c: DOUBLE EXPONENTIALLY TAPERED SLOTS

A Double Exponentially Tapered Slot Antenna (DETSA) that operated across the whole UWB has been presented in [65]. The proposed design is based on the Vivaldi structure with modifications to the slot-line conductors where the outside edge is tapered. The DETSA was built on a flexible liquid crystal polymer (LCP) organic material, allowing the antenna to be folded and used in a wearable device. A high antenna gain was observed after simulations and measurements, where 7 dBi was obtained for lower frequencies and 12 dBi for the higher frequencies. However, the antenna has a large size of 136.2×66.4 mm^2. In [66], it was shown that the performance characteristics of the DETSA, such as the directivity and electrical length, can be improved by modifying the outer edge parameters.

d: RESISTIVE LOADING

Resistive loading is another technique that has shown its ability in enhancing the bandwidth of Vivaldi antennas. By modeling the equivalent circuit of the design and analyzing

its properties, the bandwidth of a Vivaldi antenna of a size of 62 × 70 × 0.5 mm^3 was improved in [67], by adding a resistive load on the antenna and a short circuit pin. The resulting design was able to operate in the frequency range of 1 to 20 GHz and has an antenna gain that varies between 0.9 and 7.8 dBi over the frequency range.

e: CIRCULAR SLOTTED ARM STRUCTURE

A slot-loaded Vivaldi antenna with a circular shape has been presented in [68]. Each arm of the conventional design is replaced with a circular-shaped load which allows to improve the antenna bandwidth while maintaining a compact geometry. The lower frequencies can be extended by adding properly optimized slots to the circular arms. These slots also improve the antenna's radiation characteristics, such as its radiation pattern and directivity. The proposed antenna operates in the frequency range of 2 to 50 GHz and it is characterized by a suppressed sidelobe compared with a circular design without slots, and a higher antenna gain that varies between 3 and 12 dBi.

f: FRACTAL LEAF ARM STRUCTURE

A Fern Fractal Leaf structure of the Antipodal Vivaldi Antenna (AVA) was presented in [69] which offers improvements in the lower impedance bandwidth. The proposed design operates in the bandwidth of 1.3 to 20 GHz and has a size of 50.8 × 62 mm^2. Simulations were performed to evaluate the S11 parameter of the antenna, which was then compared to the measured results of the fabricated design. The simulated and measured results showed great agreement where the value of the reflection coefficient remained below −10 dB across the whole operational bandwidth.

2) MONOPOLE ANTENNA

Monopole antennas have been widely used in microwave breast imaging research. Their different shapes can be optimized and modified to achieve a wide bandwidth [70], [71]. For example, a square monopole structure has been desirable due to its ease of manufacturing and ability to support a wide range of frequencies. A square monopole antenna presented in [72] had a size as small as 10 × 10 mm^2 while operating in the frequency range of 4 to 9 GHz.

a: GROUND SLOT AND SLIT GEOMETRIES

The operational bandwidth of the square monopole structure can be significantly increased by performing some modifications to the ground plane that provide adjustments to the electromagnetic coupling effects between the radiating patch and the ground plane, without enlarging the size of the antenna. Such a case has been reported in [73] where an open circuit structure slit was cut into the ground plane of a square monopole of size 12 × 18 mm^2. In addition, the insertion of a π-shaped parasitic structure was done to the same ground plane. These modifications allowed a

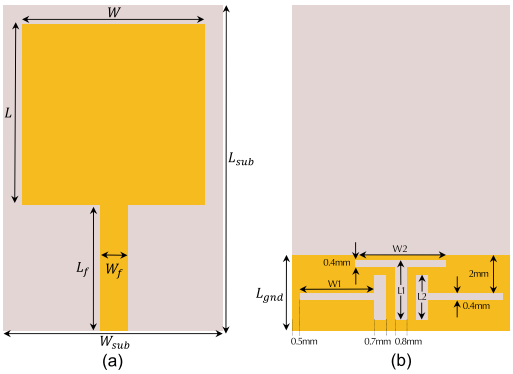

FIGURE 10. Monopole antenna: (a) top layer, (b) bottom layer, presented in [75].

130% increase in the operational bandwidth of the antenna, by extending the bandwidth from 3.12 – 10.45 GHz to 2.19 – 14.72 GHz.

Another approach is to insert a T-shaped notch into the ground plane of a square monopole antenna, which can provide a usable fractional bandwidth that exceeds 120%, as presented in [74]. The proposed antenna operates in the range of 3.12 to 12.74 GHz and has a compact size of 12 × 18 mm^2. Similarly, three T-shaped slots were inserted into the ground of a square monopole in [75] where one slot was placed between two rotated slots, as shown in Fig. 10. This design operates in a wider range of 2.96 to 15.8 GHz with a maximum gain measured to be 6.1 dBi. Another type of slots is found in [76] where E-shaped slots were used. In [77] and [78], L-shaped slits were embedded into the ground plane, concluding with similar results. A hybrid design that incorporates two different types of slot geometries is found in [79], where E-shaped slots and T-shaped strips were introduced into the ground plane of the same conventional monopole, allowing an 86% increase in the radiation efficiency over a larger bandwidth. A pair of loop sleeves were also introduced to the ground plane of a square monopole in [80], allowing the antenna to operate in the range of 3.19 to 11.03 GHz while maintaining a size of 20 × 12 mm^2.

An optimized coplanar waveguide-fed triangular planar monopole antenna was presented in [81], where rectangular notches were introduced in the ground planes to increase the impedance bandwidth to 3.05 − 12.85 GHz. The rectangular notch of dimensions $L = 4$ mm and $W = 1.25$ mm was introduced at the upper corner of each of the two finite ground planes near the radiating patch.

In [82], the operational bandwidth of two elliptical antennas was improved to span across the range of 3 to 20 GHz with the usage of ground slots. In the first design, which is of size 30 × 28 × 1.6 mm^3, two slots of 1 mm width and 9 mm length have been engraved on the back of the antenna with an orientation angle of 45 degrees. The second design is similar to the first, with the difference of a bigger slot length of 14 mm and an orientation angle of 90 degrees, in addition to a reduced substrate width of 24 mm. Simulations showed

antenna gain values that range between 7.4 to 8.84 dBi and 7.15 to 9.08 dBi for the first and second design respectively.

b: SEMICIRCULAR BASE

A shortened planar hexagonal antenna for UWB applications with an improved impedance bandwidth was presented in [83]. A semicircular base of the upper and lower side of the hexagonal radiator was utilized to increase the impedance bandwidth to $1.24 - 20$ GHz. This resulted in a higher impedance bandwidth when compared with other reported planar hexagonal antennas. Similarly, smooth transitions between resonant frequencies was ensured by tapering the base of the radiating patch to a semi-circle in [84], where the design of a coplanar waveguide-fed (CPW-fed) square monopole antenna that operates in the frequency range of 3.4 to 9.9 GHz was presented. Simulated and measured results showed good agreement, where the antenna was able to efficiently provide a stable pattern across the desired bandwidth while achieving a good impedance match in the coupling medium.

c: OCTAGONAL SHAPE

A wider operation frequency range was provided in [85], where a Modified Octagonal Shape Ultra-Wideband Monopole Microstrip Antenna (MOSUMMA) was presented. The proposed antenna operates in the range of 3 to 15 GHz while having a size of $27 \times 29 \times 1.6$ mm^3. This design is based on the basic rectangular monopole structure but features and etched out a circle in the radiating patch, a patch with a plus symbol inside the circle, and step cuts in the rectangular shape's front face. These modifications allowed to significantly increase the operational bandwidth which was validated by simulations and measurements.

3) BOWTIE ANTENNA

Shortening Strips: In [86], shortening strips were placed on the upper side of the substrate of a bowtie antenna with meandering lines, as shown in Fig. 11. The capacitive nature of the double-layered antenna with meandered lines is compensated with this modification, which also provided additional resonances. These strips allowed to enhance the bandwidth of the antenna to operate in the range of 0.85 to 3 GHz while maintaining the same size. This was validated through simulations and measurements.

4) FRACTAL ANTENNAS

a: FORK FEEDING

Using a microstrip feed line with a fork-like tuning stub is a technique that has proven its ability in enhancing the bandwidth of wide slot antennas [87]. By properly selecting the parameters of the fork-feed, coupling can be controlled between the microstrip line and the wide-slot, thus providing enhancement in the bandwidth. In [88], a wide-slot UWB antenna, shown in Fig. 12, of dimensions of $14 \times 13 \times 1.25$ mm^3, was designed using the fork feed structure which

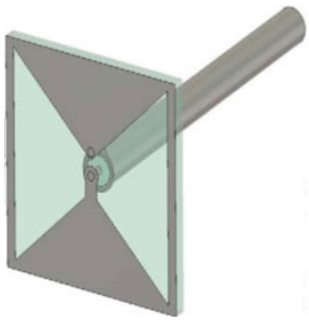

FIGURE 11. Presented bowtie antenna in [86] (©[2014] IEEE).

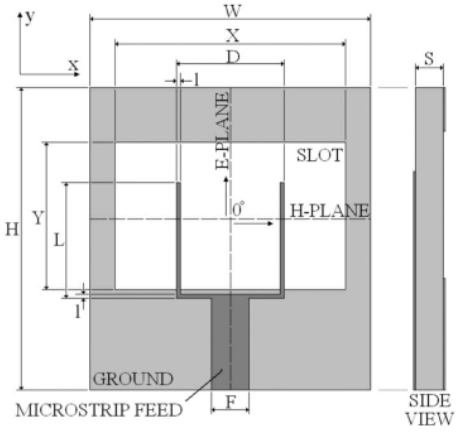

FIGURE 12. Wide-Slot antenna with a microstrip fork feed presented in [88] (©[2010] IEEE).

enhanced radiation efficiency at higher frequencies. Results showed great success where the system was able to detect tumors, possessing a diameter of 7 mm, that may be located anywhere inside the breast and up to a distance of 4 mm from the skin. Similarly, in [89], a good matching performance was achieved for a microstrip tapered slot antenna from 2 to 8 GHz by using the fork feeding line.

b: RESISTIVE LOADING

Resistive coating was placed on top of the substrate in the design of a miniaturized microstrip "Dark Eyes" antenna [90] that operates in the frequency range of 2.7 to 9.7 GHz. The added resistive layers allow the antenna to achieve a broadband behavior. Simulations and analysis of the antenna's return loss curve validated the ability of this design to operate in the desired bandwidth. The conceptual design of this antenna was later developed in [91] with the purpose of further miniaturizing the design and offering improvements in the lower operation frequency of the antenna. This resulted in a traveling wave tapered and loaded antenna (TWTLA) that operates in the frequency range of 1.9 to 35 GHz, offering an ultra-broadband operation.

c: FOURTEAR STRUCTURE

A Fourtear antenna, shown in Fig. 13, operating in the $2 - 10$ GHz range, has been presented in [92]. The effect of different antenna polarizations were shown to affect the

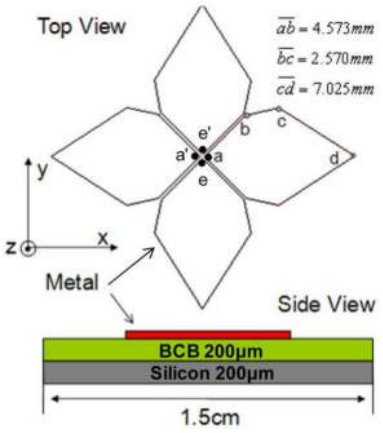

FIGURE 13. Geometry of the fourtear antenna presented in [92] (©[2008] IEEE).

performance of artificial neural networks in the statistical detection of breast cancer tumors. The proposed antenna was chosen due to its broadband characteristics. By using identical arms, the antenna was capable of operating with dual linear polarizations and was designed using two different layers of substrate made of silicon and benzo-cyclobutene (BCB) of dimensions of 15 × 15 mm^2. Simulations on a breast and tumor model were performed. Results highlighted the effect of the excited polarization and tumor orientation on the prediction success of the neural network, and showed that higher accuracy predictions may be achieved when the tumor's main axis and the polarization are parallel.

d: HIBISCUS PETAL STRUCTURE

A hibiscus petal shape of the radiating patch was shown to offer a wide bandwidth and a stable radiation pattern in [93], where the design of a microstrip antenna with a hibiscus petal pattern patch structure operating in the frequency range of 3.1 to 10.6 GHz was presented. This special structure is fed by a microstrip line, with the whole radiating patch built using RT/Duroid 5870 substrate with a dielectric constant of 2.33. Simulations were performed to evaluate the reflection coefficient of the antenna, which showed two resonance peeks at 4.5 GHz and 8.5 GHz with the whole S11 curve being below −10 dB for the desired bandwidth. These results agree well with the measured ones after fabrication of the antenna.

5) HORN ANTENNAS

A few works in the literature have also introduced the usage of horn antennas for microwave breast imaging. Such types of antennas are attractive due to their ability to support a wide bandwidth of operation [94]. Ridges can be also applied to horn antenna to enhance the operation bandwidth by extending the lower cut-off frequency of the waveguide. In [95], a double-ridged horn antenna was designed to operate in the frequency range of 1 to 6 GHz and was compared with the performance of a Vivaldi antenna in measuring reflection from a breast phantom that was used for image formation later on. It was shown that the double-ridged horn provided a higher value of tumor to fibroglandular ratio for all reconstructed images. Similarly, in [96], a pyramidal horn antenna was designed with one ridge on the lower plate and the other ridge replaced by a curved metallic launching plane on the upper plate. The curvature and shape of the plate was optimized to minimize reflections and provide good impedance matching with a coaxial feed. The obtained design was able to operate over the range of 1 to 11 GHz with a fidelity value that exceeds 0.92.

Table. 1 summarizes the different investigated antennas with bandwidth enhancement. These papers are further compared based on their performance in Table. 2.

B. MINIATURIZED SIZE

1) VIVALDI ANTENNA

a: ANTIPODAL DESIGN

The antipodal vivaldi antenna (AVA) is known to achieve a wider bandwidth and a smaller size compared with the conventional Vivaldi antenna. An AVA that operates over the UWB range of 3.1 to 10.6 GHz has been presented in [97]. The proposed design was fabricated using Rogers RT6010LM substrate and has a compact size of 52 × 52 mm^2. Results validated the capability of this design in being used for high resolution microwave imaging, where a peak gain of 10.8 dBi was measured, along with a front-to-back ratio of above 16 dB. These results came in close agreement with simulations, demonstrating the ability of the antenna to provide distortionless support for narrow pulses. Unwanted backward radiations of the AVA design were minimized in [98] by the use of resistive layers that can be placed behind the radiation layers of the antenna structure. A similar design is found in [99] where a tapered slot antenna in the form of an AVA was presented. The proposed design is also compact, having a size of 50 × 50 mm^2 and operates across the whole UWB range. Compared with [97], it has a lower antenna gain that varies between 3.5 and 9.4 dBi.

b: CORRUGATIONS

Corrugations may also be used to keep the size of the AVA compact. In [100], two steps were taken to miniaturize a microstrip-fed antipodal tapered-slot antenna to about 20% of the same antenna designed using the traditional approach. First, the microstrip feeder was directly connected to the radiator after it was curved away from the edge of the structure. Then, symmetrical corrugations of depth varying from 1 mm for inner corrugations to 3 mm for outer corrugations were introduced in the radiator and the ground plane. The final design has dimensions of 25 × 30 mm^2, compared with the original dimensions of 60 × 60 mm^2. Similarly, in [101], an AVA operating across the whole UWB range was presented. Corrugations with a depth of 4 mm, a length of 1 mm, and a spacing value of 0.5 mm, were also used to give the antenna a compact size of 22 × 40 mm^2.

TABLE 1. Investigated antennas and techniques for bandwidth enhancement.

Antenna Type	Technique	Reference	Design Type
Vivaldi Antenna	Corrugations	[60]	Uniformly Corrugated Vivaldi
		[61]	Non-Uniformly Corrugated Vivaldi
		[62]	Corrugated Vivaldi with Cavity Opening
	Balanced Design	[63] - [64]	Balanced Antipodal Vivaldi Antenna (BAVA)
	Double Exponentially Tapered Slots (DETSA)	[65] - [66]	DETSA
	Resistive Loading	[67]	Resistively Loaded Vivaldi Antenna
	Circular Slotted Arm Structure	[68]	Slot Loaded Vivaldi Antenna
	Fractal Leaf Arm Structure	[69]	Fern Fractal Leaf AVA
Monopole Antenna	Ground Slot and Slit Geometries	[73]	Square Monopole with Slits and π-shaped Parasitic Structure
		[74]	Square Monopole with T-shaped Notch
		[75]	Square Monopole with T-shaped Slots
		[76]	Square Monopole with E-shaped Slots
		[77]	Square Monopole with L-shaped Slits
		[78]	Rectangular Monopole with L-shaped Slots
		[79]	Square Monopole with E-shaped and T-shaped Slits
		[80]	Monopole Antenna with Loop-Sleeve Ground Structure
		[81]	Ground-Notched Triangular Monopole
		[82]	Ground-Slotted Elliptical Monopoles
	Semicircular Base	[83]	Shorted Planar Hexagonal Antenna
		[84]	CPW-fed Square Monopole
	Octagonal Shape	[85]	Modified Octagonal Shape Monopole Antenna (MOSUMMA)
Bowtie Antenna	Shortening Strips	[86]	Bowtie Antenna with Straight Strip Line
Fractal Antenna	Microstrip Fork Feeding	[88]	Wide-Slot Antenna
		[89]	Tapered Microstrip Slot Antenna
	Resistive Loading	[90]	Microstrip Dark Eyes Antenna
		[91]	Traveling Wave Tapered and Loaded Antenna (TWTLA)
	Fourtear Structure	[92]	Fourtear Antenna
	Hibiscus Petal Structure	[93]	Hibiscus Petal Pattern Patch Antenna
Horn Antenna	Ridges	[95]	Double Ridged Horn Antenna
		[96]	Ridged Pyramidal Horn Antenna

c: SUBSTRATE WITH A HIGH DIELECTRIC CONSTANT

When dealing with microstrip antennas, choosing a substrate with a high dielectric constant, if available, is considered the simplest solution to reduce the size of the antenna. As the permittivity of the substrate increases, the speed of wave propagation in the medium decreases, and hence the wavelength also decreases with the frequency remaining constant, as in (3),

$$\lambda_d = \frac{\lambda_0}{\sqrt{\epsilon_r}} \tag{3}$$

where λ_d is the wavelength in the dielectric substrate, λ_0 is the wavelength corresponding to the frequency of operation, and ϵ_r is the dielectric constant of the substrate. As a result, the required length of the antenna decreases, and a miniaturized design can be achieved. This is exemplified in [102] where the substrate TCream E-37 with a high dielectric constant of 37 was chosen to miniaturize the design of an AVA. The proposed antenna is of size 30 $\times$ 36 mm^2 and operates in the frequency range of 0.5 to 3 GHz.

2) BOWTIE ANTENNA

a: CROSS DESIGN

A compact size of the bowtie antenna can be obtained by using the cross design introduced in [103] where two crossed bowtie antennas of size 62.5 $\times$ 62.5 mm^2 were presented. To block any waves from radiating away from the breast, an octagonal cavity was placed behind the bowtie elements and was attached using a metal flange. Dielectric filling of a fat-like substance was placed inside the cavity to provide a better matching with the breast. The fabricated prototype of this design showed its ability of detecting elliptical tumors with a length of 1.5 cm up to a depth of 1 cm.

b: MEANDERING LINES

Miniaturization of the bowtie antenna can also be achieved by introducing meandered lines within a double-layer structure. This technique was validated in [104], where a compact double-layer bowtie antenna operating in the frequency range of 0.5 to 2 GHz has been presented. The proposed antenna was miniaturized to achieve total dimensions of 30 $\times$ 30 mm^2 and was able to operate for the same frequency

TABLE 2. Performance of the investigated antennas with bandwidth enhancement.

Ref.	Dimensions (mm)	Dielectric Material	Dielectric Constant	Frequency Band (GHz)	Results Obtained Through	
					Simulations	Measurements
[60]	260x360	FR4	4.5	1-3	✓	
[61]	50x62x1.52	Taconic RF-35	3.5	1.96-8.61	✓	✓
[62]	50x50	FR4	4.4	2.9-12	✓	✓
[63] - [64]	80x44x9.2	RT/duroid 6002	2.94	2.8-18	✓	✓
[65] - [66]	136.2x66.4	Liquid Crystal Polymer (LCP)	3.1	3.1-10.6	✓	✓
[67]	62x70x0.5	FR4	4.4	1-20	✓	✓
[68]	N/A	Rogers Duroid 5880	2.2	2-50	✓	✓
[69]	50.8x62	FR4	4.4	1.3-20	✓	✓
[72]	10x10	Rogers RO3010	10.2	4-9	✓	✓
[73]	12x18	FR4	4.4	2.91-14.72	✓	✓
[74]	12x18	FR4	4.4	3.12–12.73	✓	✓
[75]	12x18x0.8	FR4	4.4	2.96-15.8	✓	✓
[76]	12x18x1.6	FR4	N/A	2.9-15	✓	✓
[77]	12x18x1.6	FR4	N/A	2.95-14.27	✓	✓
[78]	32x35	FR4	4.6	3.1-10.6	✓	✓
[79]	12x18	FR4	4.4	2.97-12.83	✓	✓
[80]	20x25	FR4	4.3	3.19-11.03	✓	✓
[81]	24x31	FR4	4.4	3.05-12.85	✓	✓
[82]	30x28x1.6	FR4	3.9	3-20	✓	
	30x28x1.6	FR4	3.9	3-20	✓	
[83]	N/A	N/A	N/A	1.24-20	✓	✓
[84]	30x26	FR4	4.4	3.4-9.9	✓	✓
[85]	27x29x1.6	FR4	4.4	3-15	✓	✓
[86]	30x30	Rogers 6010	10.2	0.85-3	✓	✓
[88]	14x13x1.25	Rogers Duroid 6010	10.2	3-10	✓	✓
[89]	19x19	Rogers Duroid 6010 (Top Layer) & Rogers Duroid 5880 (Bottom Layer)	10.2 (Top Layer) & 2.2 (Bottom Layer)	2-8	✓	✓
[90]	22.25x20x1.3	Rogers Duroid 6010	10.2	2.7-9.7	✓	
[91]	18x14	Rogers Duroid 6010	10.2	1.9-35	✓	
[92]	15x15	Silicon & Benzocyclobutene	2.33	2-10	✓	
[93]	31x31	RT/Duroid 5870	2.33	3.1-10.6	✓	✓

range of the conventional bowtie structure with a larger size of 50 × 50 mm^2. The antenna was fabricated using Rogers RT 6010 substrate with a relative permittivity of 10.2 and was immersed in a liquid phantom for measurements. Good agreement was observed between the measured and simulated reflection coefficient results.

Table. 3 summarizes the different investigated antennas with miniaturized size. These papers are further compared based on their performance in Table. 4.

C. ENHANCED RADIATION CHARACTERISTICS

1) VIVALDI ANTENNA

a: SIDE SLOTS

Applying different shapes of slots to the sides of the conventional and antipodal Vivaldi antennas is a technique that can provide several enhancements in the radiation characteristics of these antennas. Six side slots were applied to the regular Vivaldi antenna in [105], where the final design provided a pattern with better directivity compared with the conventional design, as well as a higher antenna gain. These improvements can be offered merely by introducing the side slots and would not affect the size of the antenna, which is desired to be as miniaturized as possible. The final design was able to operate in the frequency range of 1.54 to 7 GHz with a radiation efficiency of 92%. Hemi-cylindrical slots were introduced to a Vivaldi antenna in [106], allowing to improve the antenna gain, front-to-back ratio (FBR), impedance matching, and cross-polarization discrimination (XPD). The proposed design was able to operate in the range of 2.9 to more than 9 GHz with a peak gain of 9.5 dBi while maintaining a size of 49 × 48.5 × 0.8 mm^3.

In [107], an improvement of the gain of an antipodal linearly tapered slot antenna (ALTSA) with unequal half-circular slots embedded on both edge-sides was presented. This antenna, which operates at 3.1 GHz to more than 10.6 GHz, showed narrow 3 dB beamwidths since the slots can change the edge surface current. Its gain was improved by up to 3.5 dB when compared with a reference ALTSA.

In [108], periodic slit edges were applied to the conventional AVA design with a trapezoid-shaped dielectric lens to improve its radiation characteristics, by extending the lower frequency range while also increasing the antenna gain. In later work [109], the same group further improved their

TABLE 3. Investigated antennas and miniaturization techniques.

Antenna Type	Technique	Reference	Design Type
Vivaldi Antenna	Antipodal Design	[97]	Antipodal Vivaldi Antenna (AVA)
		[98]	Tapered Slot AVA
		[99]	Tapered Slot AVA
	Corrugations	[100]	Corrugated Tapered Slot AVA
		[101]	Corrugated Tapered Slot AVA
	Substrate With a High Dielectric Constant	[102]	AVA
Bowtie Antenna	Cross Design	[103]	Crossed Bowtie Antenna
	Meandering Lines	[104]	Double-Layered Bowtie Antenna

TABLE 4. Performance of the investigated miniaturized antennas.

Ref.	Dimensions (mm)	Dielectric Material	Dielectric Constant	Frequency Band (GHz)	Results Obtained Through	
					Simulations	Measurements
[97]	52x52	Rogers RT6010LM	10.2	3.1-10.6	✓	✓
[98]	50x50	Rogers RO4003C	3.38	3.1-10.6	✓	✓
[99]	59.6x59.9	Rogers RT6010LM	10.2	3.1-10.6	✓	✓
[100]	25x30	Rogers RT6010	10.2	1.8-10.8	✓	✓
[101]	22x40	Rogers RT6010	10.2	3.1-10.6	✓	
[102]	30x36	TCream E-37	37	0.5-3	✓	
[103]	62.5x62.5	N/A	N/A	2-4	✓	✓
[104]	30x30	Rogers RT6010	10.2	0.5-2	✓	✓

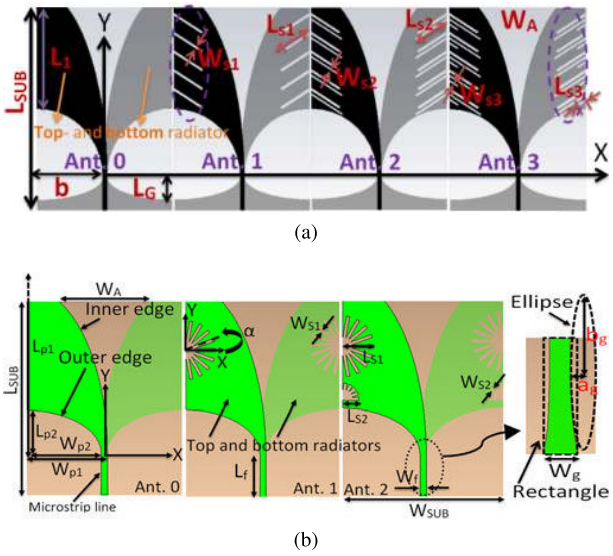

FIGURE 14. Modifications of Vivaldi antenna: (a) original design [108] (©[2016] IEEE), (b) modified design, presented in [109] (©[2017] IEEE).

proposed design by using rectangular slits resulting in a final design that provided a gain larger than 10 dBi across the whole operating range of 10 to 50 GHz, with size reduction of 40% reaching final dimensions of 30×55 mm^2. An elliptical-shaped dielectric lens was also applied in this design, offering an improved front-to-back ratio, elevated gain values at high frequencies, lower sidelobes in the radiation pattern, as well as lower cross-polarization levels. Both designs are shown in Fig. 14.

Regular slot edges (RSE) were introduced to the design of an AVA in [110], allowing to extend the lower frequency of the by 9% without altering the size of the antenna. The resulting RSE AVA was shown to have a return loss below -10 dB from 4 to 30 GHz. The problem of distortions that occur in the radiation pattern of the antenna and the decrease in the antenna gain at higher frequencies were reduced by the introduction of a curved lens that can offer gain enhancement and stability in the radiation pattern. This was validated by simulations and measurements which showed an increase in the antenna gain by a maximum of 7 dB at 23 GHz and 1 dB at 13 GHz. Exponential slot edges (ESE) were applied to an AVA in [111], giving the antenna a palm tree structure that allows the extension of the low-end bandwidth, reducing the side lobe levels (SLL) and back lobe level, in addition to increasing the antenna gain in the main lobe. Compared to a regular AVA, the ESE-AVA was able to reach a gain of 8.3 dBi and a SLL of -15 dB in an operational bandwidth from 5.6 to 11 GHz. Similar ESEs were applied to the design of a BAVA in [112] with a curving dielectric director, allowing to improve its gain to a value of 12.6 dBi. More improvements were obtained in [113], where a tapered slot edge (TSE) design was used in an AVA resulting in a wider bandwidth. The TSE-AVA operates from 2.4 to more than 14 GHz with a peak gain of 10 dBi at 7 GHz while maintaining a compact size of 48×60 mm^2.

b: DIELECTRIC LENS

To improve the radiation pattern and cross-polarization of a conventional BAVA, where a tilted beam is usually obtained at higher frequencies, a dielectric lens (DL) is introduced in [114] to the front of the antenna's aperture. The DL helps in increasing the path length and retarding the passing wave, thus causing it to collimate. This offers a more directive pattern and a higher antenna gain. The proposed DL-BAVA was

TABLE 5. Investigated antennas and techniques for radiation characteristics enhancement.

Antenna Type	Technique	Reference	Design Type
Vivaldi Antenna	Side Slots	[105]	Side Slotted Vivaldi Antenna
		[106]	Hemi-cylindrical Slotted Vivaldi
		[107]	ALTSA
		[109]	AVA with Rectangular Slits
		[108]	AVA with Periodic Slit Edge
		[110]	AVA with Regular Slot Edges (RSE-AVA)
		[111]	AVA with Exponential Slot Edges (ESE-AVA)
		[113]	AVA with Tapered Slot Edge (TSE-AVA)
		[112]	ESE-BAVA
	Dielectric Lens	[114]	DL-BAVA
		[115]	Modified BAVA
	Reflector Structure	[116]	Cavity-Backed Vivaldi Antenna
Monopole Antenna	Parabolic-Shaped Ground	[117]	Monopole Antenna with Parabolic-Shaped Ground Plane
	Reflector Structure	[40]	Elliptical Monopole with Reflector
Bowtie Antenna	Resistive and Capacitive Loading	[118]	Modified Wire Bowtie Antenna
		[119]	Resistively Loaded Bowtie Antenna
		[120]	RC-Loaded Bowtie Antenna
	Slotline	[121]	Slotline Bowtie Hybrid Antenna
Horn Antenna	Dielectric Shielding	[89]	TEM Horn Antenna
		[122] - [123]	TEM Horn Antenna

capable of operating in the frequency range of 3 to 18 GHz with a better return loss value compared with the regular BAVA. Additionally, a bore-sight gain higher than 10 dBi was achieved, which is an improvement on the conventional BAVA where the gain does not exceed 10 dBi. Modifications to the shape of the substrate were proposed in [115] to act as a DL, where similar results in the radiation pattern can be obtained without the need to incorporate a separate lens to the antenna.

c: REFLECTOR STRUCTURE

The antenna gain of conventional Vivaldi antennas was improved by the cavity-backed design introduced in [116], where a carefully-designed reflector structure was incorporated with the antenna. The cavity-backed Vivaldi antenna (CBVA) was designed to operate in the frequency range of 2.5 to 8.5 GHz. By measurements and simulations, the CBVA proved to have multiple improvements in the radiation characteristics compared with a regular Vivaldi, most notably by an increase of 2.1 dBi in the peak antenna gain and an 8.5 dB decrease in the front-to-back ratio.

Table. 5 summarizes the different investigated antennas with bandwidth enhancement. These papers are further compared based on their performance in Table. 6.

2) MONOPOLE ANTENNA

a: REFLECTOR STRUCTURE

An elliptical shape was chosen in [40] to offer a compromise between the wide bandwidth provided by the rectangular monopole and the pattern stability found in circular monopoles. The elliptical monopole is of size 24×33.5 mm^2 and operates in the frequency range of 1 to 4 GHz. To improve the directional properties, a reflector was used and positioned behind the antenna, resulting in reduced back-radiations at the expense of a larger antenna size of 60×60 mm^2 and a slightly reduced impedance match. However, the improved transmission response was proven in both simulated and measured results that showed a S21 curve above -60 dB from 1 to 4 GHz.

b: PARABOLIC SHAPED GROUND

In [117], a directional monopole antenna with an improved directivity and a stable directional radiation pattern was presented by introducing a modified ground plane with a parabolic shape. The axis of the parabolic shape was extended throughout the direction of the substrate diagonal and parabolic-shaped slots were inserted at the corners of the ground plane to reach an improved directivity of 5-15 degrees. It was shown through both simulations and measurements that the antennas had a stable radiation pattern and in the bandwidth of 4 to 9 GHz an improved gain of $1.3-3.1$ dB.

3) BOWTIE ANTENNA

a: RESISTIVE AND CAPACITIVE LOADING

To minimize the late ringing time of the bowtie antenna, which are caused by internal reflections, resistive loadings may be used to achieve consistent pulse radiation. This loading may be optimized for minimal end reflections [118], [124]. Such a design has been reported in [119], where a resistively loaded bowtie antenna of dimensions of 70.3×37 mm^2 operating in the frequency range of 3.3 to 10 GHz was presented. The resistive loading consists of six resistors optimized using a genetic optimization algorithm. To validate this design, simulations of the near field distributions at 4, 6, and 8 GHz were performed and showed good agreement with the measured results. A similar study is found in [120]

TABLE 6. Performance of the investigated antennas with enhanced radiation characteristics.

Ref.	Dimensions (mm)	Dielectric Material	Dielectric Constant	Frequency Band (GHz)	Results Obtained Through	
					Simulations	Measurements
[105]	88x75	Rogers RT/duroid 5870	2.33	1.54-7	✓	✓
[106]	49x48.5x0.8	FR4	4.3	2.9-9	✓	✓
[107]	52x145	RT/Duroid 5880	2.2	3.1-10.6	✓	✓
[109]	30×55×0.508	Rogers RO4003C	3.38	5-50	✓	✓
[108]	40x90x0.508	Rogers RO4003C	3.38	3.4-40	✓	✓
[110]	66.4x50	N/A	4.5	4-30	✓	✓
[111]	36.3x59.81	Rogers RO3206	6.15	5.6-11	✓	✓
[113]	48x60	FR4	4.6	2.5-14	✓	✓
[112]	70x140x3	ARLON Diclad880	2.2	1.5-15	✓	✓
[114]	96x50x3.15	Arlon AD255	2.55	3-18	✓	✓
[115]	105x56	N/A	2.5	6-20	✓	
[116]	63x51x1	FR4	4.4	2.5-8.5	✓	✓
[117]	50x50	FR4	4.4	4-9	✓	✓
[40]	24x33.5	Taconic CER-10	9.8	1-4	✓	✓
[118]	23x7	FR4	4.4	0.42-1.67	✓	✓
[119]	70.3x37	N/A	N/A	3.3-10	✓	✓
[120]	N/A	N/A	N/A	0.5-5.1	✓	✓
[121]	N/A	Rogers RT6010LM	10.2	2.5-9	✓	✓

where a combination of resistive and capacitive loadings was applied to the design of a bowtie antenna. A constant resistive load was maintained along the antenna with a capacitive load that increases linearly towards the ends of the antenna. This combined loading scheme improved the pulse radiation by 54% and maintained a late ringing time below −40 dB compared with a similar bowtie antenna without loading.

b: SLOTLINE

Internal reflections of the antenna may also be reduced by introducing a slot to the structure, such as done in [121], where a slotline bowtie hybrid antenna (SBH) that operates in the frequency range of 1 to 10 GHz has been presented. The design was fabricated and tested on breast phantom material to evaluate the effect of the tumor depth on the reflection coefficient. The presented results showed that the amplitude of the reflections decreased by approximately 10 dB after an increase of 1 cm in the depth of the tumor.

4) HORN ANTENNAS

a: DIELECTRIC SHIELDING

A dielectric shield was used in [125] to enclose a TEM horn antenna, and hence block any possible electromagnetic interference that may occur from its surroundings. The proposed horn operates in the UWB range and possesses better radiation efficiency compared with regular designs, which was validated through simulations by a lower reflection coefficient value across the whole bandwidth. Similarly, in [122], [123], a TEM horn was placed in a solid dielectric medium. Copper sheets were placed on the top, bottom, and sides of the antenna resulting in a better radiation efficiency, blocked interference, improved coupling efficiency, and good impedance matching. Apertures were also introduced in the top sheet of the shield, providing a uniform field distribution.

Table. 5 summarizes the different investigated antennas with enhanced radiation characteristics. These papers are further compared based on their performance in Table. 6.

V. ANTENNA ARRAYS PROPOSED FOR MICROWAVE BREAST IMAGING

After investigating the antenna designs proposed for microwave breast imaging, the different antenna arrays found in the literature are presented in this section. We classified these arrays based on their configuration or structure which include planar, enclosed structures, and hemispherical. The performance of the investigated arrays is summarized at the end of this section in Table. 7, where they can be compared according to some of their major characteristics including: the methods adopted to obtain measurements, which include monostatic, bistatic, and multistatic methods, the array operating frequency band, the design of the antenna elements, and their total number in the investigated array.

A. PLANAR ARRAYS

The earliest antenna array proposed for microwave breast imaging is a 2 × 2 bowtie planar antenna with resistive profiles, presented for breast cancer detection in [126]. The antennas were printed on a lossy substrate that can help in decreasing the mutual coupling and increasing the operating bandwidth. Scanning of the breast required rotating the antenna to increase the amount of information received and improve the accuracy of the detection process. The array has total dimensions of 94 × 49 mm^2, with each element fed by a coaxial transmission line. The antenna has not been fabricated, and the study investigated the simulated results.

In [127], two antenna arrays designed for microwave breast imaging have been proposed. The same antenna design has been used for both arrays. Each array consists of two antennas, and the two arrays differ according to the polarization.

TABLE 7. Investigated antenna arrays with their major characteristics.

Ref.	Array Configuration	Measurements	Operating Band	Antenna Design	Nb of Antennas	Image Reconstruction Algorithm
[126]	Planar	Monostatic	1.6–11.4 GHz	Resistively Loaded Bowtie	4	N/A
[127]	Planar	Monostatic	3.1–10 GHz	Slot patch	2	N/A
[128]	Planar	Monostatic	3.5–15 GHz	Slot Monopole	16	N/A
[129]	Planar	Monostatic or Bistatic	2–16 GHz	Monopole	2	DAS
[130]	Enclosed Cubical	Multistatic	0.5–3 GHz	Slot patch	32	Distorted Born Iterative Method (DBIM)
[131]	Enclosed Cubical	Multistatic	0.5–3 GHz	Slot patch	32	N/A
[133]	Enclosed 12-sided cavity	Multistatic	Design 1: 2.75 GHz Design 2: 915 MHz	Bowtie	36	Born Iterative Method (BIM)
[135], [137]	Hemispherical	Multistatic	4.5–10 GHz	Cavity backed aperture stacked patch antenna	16	Modified DAS
[136]					31	Modified DAS
[138]	Hemispherical	Multistatic	1.2–7 GHz	Modified Bowtie	16	IDAS
[139], [140]	Hemispherical	Multistatic	2–4 GHz	Monopole & Spiral	16	DAS

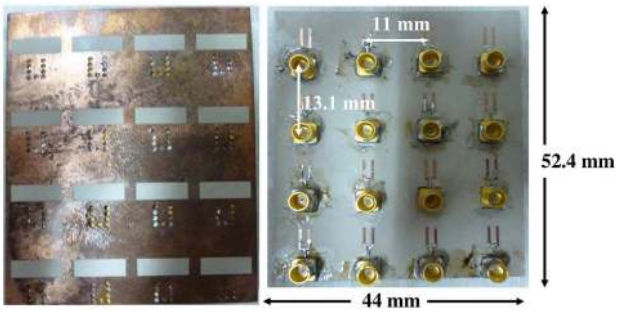

FIGURE 15. Proposed Planar array: (a) back side, (b) front side, presented in [128] (©[2013] IEEE).

To study the effect of received signal polarization on the detection accuracy, two different configurations have been studied, one with co-polarization, and the second with cross-polarization. The antenna element is a slot patch, operating from 3.1 to 10 GHz. It was shown that the co-polarized configuration performs better in detecting tumors away from the chest wall, whereas the cross-polarized configuration is preferred in detecting tumors close to the chest wall. The antennas have been tested in two different measurements setups, one with pork fat, and the second with pork muscle, both with a phantom mimicking the tumor.

In [128], an UWB planar 4 × 4 array, shown in Fig. 15, has been also presented for microwave breast imaging. Each antenna element is made of a monopole slot antenna with a miniaturized size. Duroid RT with a relative permittivity of 10.2 has been used as a substrate. The antenna dimensions have been optimized using a stack of dielectric materials of 40 mm thickness placed below the antenna that can mimic the skin and adipose. The whole antenna array operated from 3.5 to 15 GHz. Homogenous and inhomogeneous breast phantoms along with a glandular phantom have been used in the measurements and in the 3D confocal imaging. It has been shown that the proposed system was able to detect a tumor of 10 × 10 × 1 mm^3 size with a 10 mm separation distance.

In [129], an integrated system proposed for microwave imaging system has been presented. A planar antenna array formed by a pair of patch antennas has been used with CMOS technology. The antenna array operated from 2 to 16 GHz using a combined circular and rectangular shape in the patches. Roger RO4003c with a permittivity of 3.55 has been used as a substrate. It was shown through experiments with breast and tumor phantoms that the proposed system can detect tumors with a resolution of 3 mm. The paper also discussed the procedure done in implementing the CMOS at the receiver side.

B. ENCLOSED ARRAYS

The second type of arrays is that formed by an enclosed array. In [130], an enclosed array in a cubical structure has been presented. The array was made of miniaturized multiband patch antennas, surrounded by a conducting enclosure. The enclosed configuration has an elliptical shape opening in the top panel that permits the patient to extend her breast through the opening, as shown in Fig. 16. A dielectric material of relative permittivity of 6.15 was used to coat the four lateral panels, having eight slot antenna elements on each panel, arranged in an optimized configuration to reduce the mutual coupling, with a total of 32 antennas. The slot in each element was used to decrease the operating frequency to a lower range from 0.5 to 3.5 GHz with a miniaturized size. Each patch antenna has a total size of 30 × 28 mm^2, spaced horizontally and vertically by 48 mm from the nearest antenna element. An immersion medium has been also used to fill the interior volume of the array, with dielectric properties that match the coupling safflower oil properties usually used in such systems. The whole system operated at 1.60, 2.20, and 3.02 GHz. The validation of the proposed system has been done through simulations.

In a continuation of their work in [130], the same group presented in [131] an improved design of the antenna patches to be used in their enclosed structure, as shown in Fig. 16b. The improved antenna element has a miniaturized size relative to its resonance frequencies operating at 1.36, 1.74, and

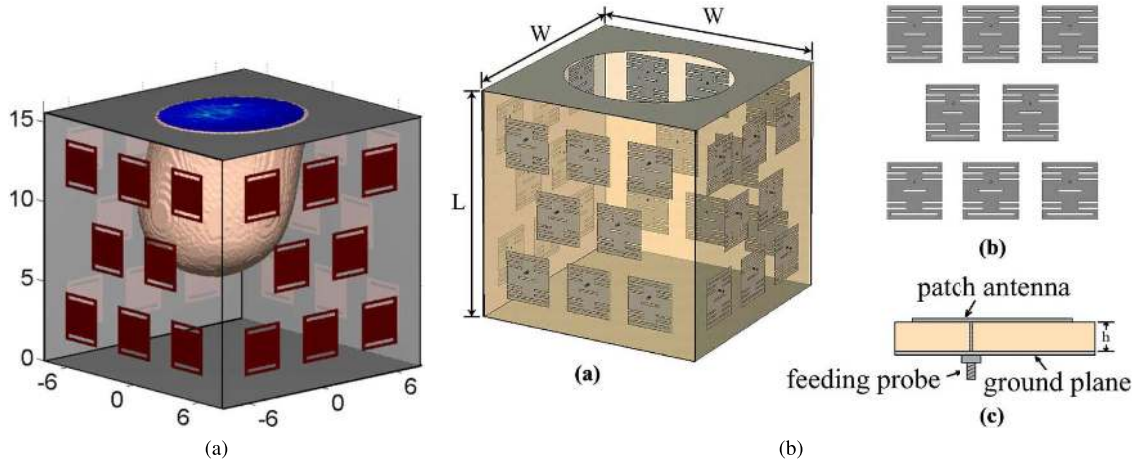

(a) (b)

FIGURE 16. Enclosed array of 32 antennas: (a) original array [130] (©[2012] IEEE), (b) improved antenna element design [131] (©[2013] IEEE).

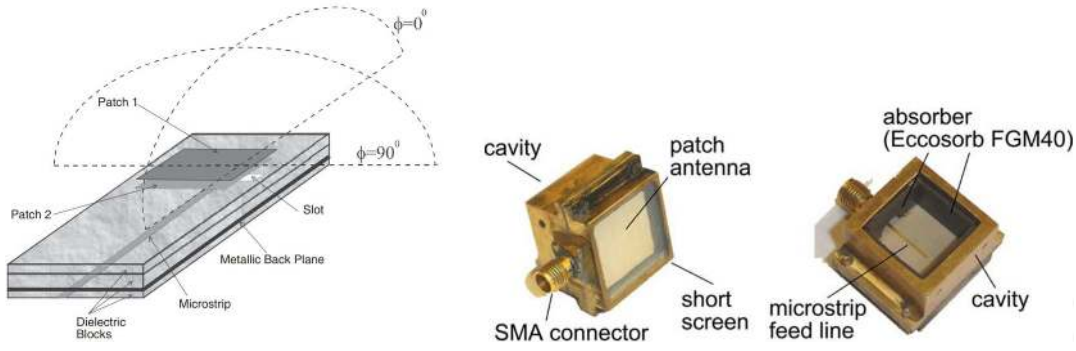

(a) (b)

FIGURE 17. Cavity backed aperture stacked patch antenna: (a) original array [134] (©[2007] IEEE), (b) improved antenna element design [135] (©[2009] IEEE).

3.03 GHz. The improvement has been made through adding additional slots in the patch antenna design. The images constructed using the whole array system were compared to those resulting from simulated array measurements using a realistic breast phantom, where good agreement has been seen.

The enclosed configuration of [130] has been also presented in [132] to protect the imaging system from external interference, but with a single operating frequency rather than the dual band operation presented in [130]. In [133], the array has the shape of a 12 sided polygon, with each panel containing three bow-tie antennas, in a total of 36 antennas. The enclosed system is also filled with a coupling liquid. It was shown, through experiments and simulations, that images can be successfully formed in the cavity geometry using the numerical characterization of the incident fields and, and the link between the incident fields and the inverse scattering algorithm resulting from the vector Green's function formulation. In addition, the location and permittivity of the object tested can be also detected.

C. HEMISPHERICAL ARRAYS

One of the earliest hemispherical array systems, have been investigated with real experimental data assessment in [27], [135], [137]. In [135], an UWB conformal hemispherical array designed for breast cancer detection has been presented. The antenna used as the element array is a modified version of the cavity backed aperture stacked patch antenna presented in [134], both shown in Fig. 17.

A modified version of the antenna presented was used in [135] in a conformal hemispherical array, shown in Fig. 18, rather than the typical planar array. The antenna element was made of two stacked patches, previously presented by the authors in [137] with the first patch being a typical rectangular patch antenna. Both patches were separated from the ground by stacked substrates: one with a relative permittivity of 2.2, and the second with relative permittivity of 10.2. A cavity backed aperture, with optimized dimensions of 23×29 mm^2 with 17 mm long, was also used to protect the antenna from the surroundings, lined with a back radiation absorber. To decrease the mutual coupling between the adjacent elements, a short metallic screen was included on the front face of the antenna, which was matched between 4.5 and 10 GHz. The antenna has been fabricated and tested, with 20 female volunteered in the fabrication process to detect the needed size of the total array to fit different breast sizes. The antennas were immersed in a matching medium to

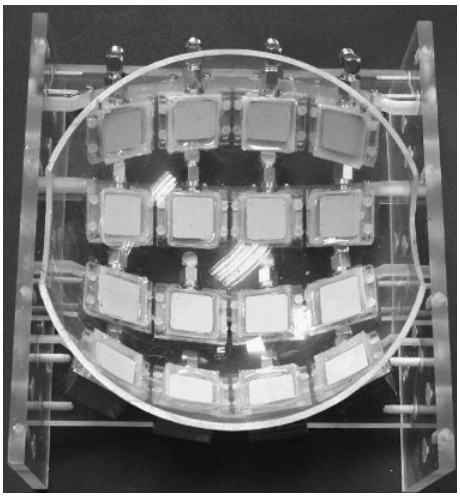

(a)

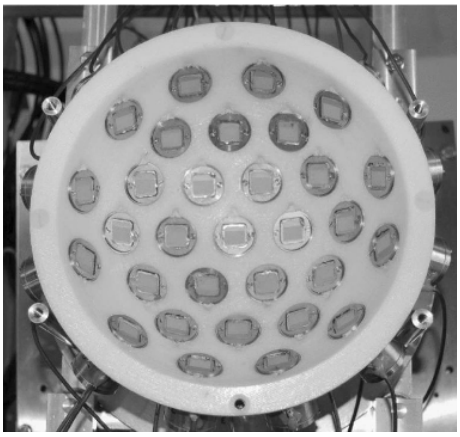

(b)

FIGURE 18. Hemispherical constructed array: (a) original array [135] (©[2009] IEEE), (b) modified array [136] (©[2010] IEEE).

attenuate the reflections from the breast skin. The measurements needed around 3 minutes to complete 120 independent measurements. Spherical tumors with diameter of 4 and 6 mm have been detected within a breast phantom of a relative permittivity of 9.8.

A later work by the same group has been presented in [136] with 2:1 low dielectric contrast between tumor and normal tissues. The improved array was made from wide-slot UWB antennas [88], previously investigated in Section IV-A4.a, and shown in Fig. 12. Since the total dimensions of this antenna was smaller than the one in [135], 31 elements were used here instead of the 16 elements in the previous design, as shown in Fig. 18b. As in [135], each antenna element was fed through coaxial cables. Comparing the 2D and 3D images of the newly designed system with the previously presented one, the 31 system array showed better results with higher accuracy and less clutter. The authors also compared having only 16 elements with their previously presented array of 16 elements. The results also showed better performance. Nevertheless, this system also needed to be filled with an

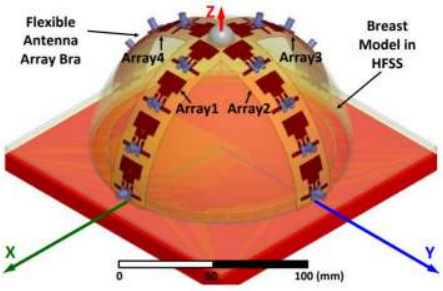

(a)

(b)

FIGURE 19. Flexible antenna array: (a) original array configuration [139] (©[2015] IEEE), (b) wearable prototype [140] (©[2016] IEEE).

immersion matching medium to attenuate the reflections from the breast skin.

In [138], a hemispherical UWB antenna array of 16 miniaturized bowtie antennas has been proposed for microwave imaging. The system operates from 1.2 to 7 GHz, with the two arms of the bowtie antenna short connected to miniaturize its size relative to its operating frequency range. The total dimensions of each antenna element was 15×15 mm^2. The antenna has been fabricated and tested, and then used in an array of hemispherical configuration to test the performance of the proposed system. Two different experiments have been conducted with breast phantoms, with one and two embedded tumors. It was shown multiple tumors, in both horizontal and vertical planes, can be detected by the proposed systems. The tumors had the sizes of 10 and 15 mm respectively, located at a depth of 18 and 30 mm inside the breast phantom.

To remedy some of the drawbacks of the arrays presented for microwave imaging related to the use of the immersion liquid, the bulkiness of some arrays, and the need to rotate either the antenna or the breast in most of these systems, a flexible array for microwave breast cancer detection has been presented by the same group in [139], [140], shown in Fig. 19.

In [139], single and dual-polarization flexible UWB antenna arrays have been presented in [139], with the array configuration shown in Fig. 19a. Kapton polyimide of relativity permittivity of 3.5, known for its flexibility and biocompatibility, was used in the design and fabrication of antennas, which makes them easier to be used with wearable applications. Each antenna array is made of two flexible 4×4 antenna elements, covered with a superstrate similar to the substrate for full biocompatibility. In order to be able to fit

this number of antennas, the antenna elements in both arrays have been miniaturized to total dimensions of 20×20 mm^2. The antenna element in the single polarization antenna array was a monopole antenna, and that of the dual-polarization antenna array is a spiral antenna. The two designs operate in the $2 - 4$ GHz band. The designed antennas have been also fabricated and tested using a breast phantom, and the results showed good agreement with the simulated ones, with good impedance matching. It has been also shown that, using a reflector, the penetration of the electromagnetic waves inside the body can be also improved. Also, the maximum power that can be used to transmit the waves from these antenna as per the ASAR was also calculated and found to be 4 mW and 3.1 mW, for the single and dual-polarization antenna arrays presented. The coupling between the different elements was not discussed in the paper.

In a continuation for the work done in [139], the same group tested their designed antennas as a wearable system in the form of a bra on a healthy volunteer over a period of 28 days in [140], and compared their wearable system to the typical table-based one in [141]. The wearable prototype is shown in Fig. 19b. It was shown that the wearable system improved the quality of collected data, with a direct contact to the skin, without the need for an immersion gel as in the table-based systems. It was also a cost-effective system with a smaller footprint.

VI. QUALITATIVE EVALUATION & DISCUSSION

A. ANTENNA ELEMENTS

The different investigated papers, presented in IV, are compared based on their bandwidth, size, design complexity, and cost of manufacturing, in Table. 8. Assuming the desired characteristics is to have a wide frequency of operation that covers the whole UWB range from 3.1 to 10.6 GHz, a compact size that does not exceed 50×50 mm^2, a simple design procedure and structure, and a low manufacturing cost, the following remarks can be concluded:

- Vivaldi antenna designs presented in [61], [65], [67]–[69] provide a wide bandwidth but suffer from a large antenna size and complex design procedure, making them unattractive for array systems. Among the investigated Vivaldi antennas, the antipodal Vivaldi antenna designs in [97]–[99] and side-slotted AVA designs in [108], [109] are found suitable for microwave imaging array systems, as they offer a smaller size compared to the other Vivaldi antennas while exhibiting a broadband behavior.
- Monopole antenna design presented in [73]–[82] satisfy the assumed design criteria by simply performing small modifications into the ground plane, making them also suitable for usage in arrays. Other monopole designs, such as [85], [117], are found not suitable due to their design complexity and large size.
- Bowtie antenna designs presented in [86], [103], [104], [118]–[121] provide a narrower band that do not span the whole UWB range, for this they were found not suitable for microwave imaging array systems.
- Other microstrip antenna, such as the fourtear [92] and wide-slot [88], are found suitable, while [90], [91], [93] are not due to their design complexity.
- Horn antennas presented in [95], [96], [122], [123], [125] offer a wide bandwidth, but they suffer from a large volume and have a higher manufacturing cost than microstrip antennas, making them unattractive choices for microwave imaging array systems.

As a conclusion, among all investigated antennas, the antipodal Vivaldi antenna designs in [97]–[99], [108], [109] and the ground-slotted monopoles in [73]–[82] stand out as the most suitable and attractive antennas for being used in antenna arrays for microwave breast imaging. The presented antipodal Vivaldi antenna designs typically operate from 3 to 10.6 GHz, and the presented ground-slotted monopoles operate from 3 to 14 GHz. Although both of these modified versions of the Vivaldi antenna and monopole antenna offer a wide bandwidth that covers the UWB range, these AVA design has a larger size when compared with the monopoles. The investigated AVA sizes range from 50×50 mm^2 to 60×60 mm^2, while monopoles can achieve a size as small as 12×18 mm^2 while also operating in the UWB range.

B. ANTENNA ARRAY CONFIGURATIONS

The different investigated papers, presented in V, are compared based on their design complexity, flexibility, biocompatibility, and cost, in Table. 9. The following remarks are found.

In conventional microwave breast imaging, the antennas are either moved with respect to the scanned breast, or the breast is moved with respect to the antennas. These systems are mainly known as static systems, which require scanning of the antenna locations to reach the optimized position for better accuracy. In contrast, multistatic systems rarely require this scanning, due to the larger number of collected signals using well-distributed antennas, but rely on the array configuration.

Typically, the array configurations found in the literature can be planar, enclosed, or hemispherical arrays. The planar arrays [126]–[129] are easier to design and fabricate, and have the advantage of simple and fast enhancement in their configuration if more antennas are required to be added, or even if it is needed to vary the separating distance between the antenna elements. However, for optimal microwave illumination, these antennas typically require to be held perpendicular to the tangent of the breast surface. In addition, the location of the antennas might require scanning for the optimized position for more accurate measurements. For this, enclosed arrays [130], [131], [133] and hemispherical arrays [27], [135]–[140] have been proposed in the last years. These systems have the advantage of fixing the antenna array and inserting the breast inside the antenna array, and use multistatic measurements. However, as a result of the enclosed

TABLE 8. A taxonomy of research that proposes antennas for microwave breast imaging.

Ref.	Proposed Design	Wide Bandwidth	Compact Size	Simple Design	Low Cost	Suitability for Array Systems
[60]	Uniformly Corrugated Vivaldi	×	×	✓	✓	×
[61]	Non-Uniformly Corrugated Vivaldi	×	✓	×	✓	×
[62]	Corrugated Vivaldi with Cavity Opening	✓	✓	×	✓	×
[63] - [64]	BAVA	✓	×	✓	✓	×
[65] - [66]	DETSA	✓	×	✓	✓	×
[67]	Resistively Loaded Vivaldi Antenna	✓	×	×	✓	×
[68]	Slot Loaded Vivaldi Antenna	✓	×	×	✓	×
[69]	Fern Fractal Leaf AVA	✓	×	×	✓	×
[97]	AVA	✓	✓	✓	✓	✓
[98]	Tapered Slot AVA	✓	✓	✓	✓	✓
[99]	Tapered Slot AVA	✓	✓	✓	✓	✓
[100]	Corrugated Tapered Slot AVA	✓	✓	×	✓	×
[101]	Corrugated Tapered Slot AVA	✓	✓	×	✓	×
[102]	AVA	×	✓	✓	✓	×
[105]	Side Slotted Vivaldi Antenna	×	×	×	✓	×
[106]	Hemi-cylindrical Slotted Vivaldi	×	×	×	✓	×
[107]	ALTSA	✓	×	×	✓	×
[109]	AVA with Rectangular Slits	✓	✓	×	✓	✓
[108]	AVA with Periodic Slit Edge	✓	✓	×	✓	✓
[110]	RSE-AVA	✓	×	×	✓	×
[111]	ESE-AVA	×	✓	✓	✓	×
[113]	TSE-AVA	✓	✓	×	✓	×
[112]	ESE-BAVA	✓	×	×	✓	×
[114]	DL-BAVA	✓	×	×	✓	×
[115]	Modified BAVA	✓	×	×	✓	×
[116]	Cavity-Backed Vivaldi Antenna	×	×	✓	✓	×
[72]	Square Monopole Antenna	×	✓	✓	✓	×
[73]	Square Monopole with Slits and π-shaped Parasitic Structure	✓	✓	✓	✓	✓
[74]	Square Monopole with T-shaped Notch	✓	✓	✓	✓	✓
[75]	Square Monopole with T-shaped Slots	✓	✓	✓	✓	✓
[76]	Square Monopole with E-shaped Slots	✓	✓	✓	✓	✓
[77]	Square Monopole with L-shaped Slits	✓	✓	✓	✓	✓
[78]	Rectangular Monopole with L-shaped Slots	✓	✓	✓	✓	✓
[79]	Square Monopole with E-shaped and T-shaped Slits	✓	✓	✓	✓	✓
[80]	Monopole with Loop-Sleeve Ground Structure	✓	✓	✓	✓	✓
[81]	Ground-Notched Triangular Monopole	✓	✓	✓	✓	✓
[82]	Ground-Slotted Elliptical Monopole with Oriented Slots	✓	✓	✓	✓	✓
	Ground-Slotted Elliptical Monopole with Vertical Slots	✓	✓	✓	✓	✓
[83]	Shorted Planar Hexagonal Antenna	✓	✓	✓	✓	✓
[84]	CPW-fed Square Monopole	×	✓	×	✓	×
[85]	MOSUMMA	✓	✓	×	✓	×
[117]	Monopole with Parabolic-Shaped Ground Plane	×	×	×	✓	×
[40]	Elliptical Monopole Antenna	×	✓	✓	✓	×
[103]	Crossed Bowtie Antenna	×	×	✓	✓	×
[104]	Double-Layered Bowtie Antenna	×	✓	✓	✓	×
[86]	Bowtie Antenna with Straight Strip Line	×	✓	✓	✓	×
[118]	Modified Wire Bowtie Antenna	×	✓	×	✓	×
[119]	Resistively Loaded Bowtie Antenna	✓	×	×	✓	×
[120]	RC-Loaded Bowtie Antenna	×	×	×	✓	×
[121]	Slotline Bowtie Hybrid Antenna	×	×	✓	✓	×
[88]	Wide-Slot Antenna	✓	✓	✓	✓	✓
[89]	Tapered Slot Antenna	×	✓	✓	✓	×
[90]	Microstrip Dark Eyes Antenna	✓	✓	×	✓	×
[91]	TWTLA	✓	✓	×	✓	×
[92]	Fourtear Antenna	✓	✓	✓	✓	✓
[93]	Hibiscus Petal Pattern Patch Antenna	✓	✓	×	✓	×
[95]	Double Ridged Horn Antenna	×	×	×	×	×
[96]	Ridged Pyramidal Horn Antenna	✓	×	×	×	×
[125]	TEM Horn Antenna	✓	×	×	×	×
[122] - [123]	TEM Horn Antenna	✓	×	×	×	×

TABLE 9. A taxonomy of research that uses antenna arrays for microwave breast imaging.

Paper	Wide Bandwdith	Simple Design	Low Cost	Flexibility	Biocompatibility
[126]	✓	×	✓	×	×
[127]	✓	✓	✓	×	×
[128]	✓	✓	✓	×	×
[129]	✓	✓	✓	×	×
[133]	×	✓	✓	×	×
[130]	✓	✓	✓	×	×
[131]	✓	✓	✓	×	×
[135], [137]	✓	×	×	×	×
[136]	✓	✓	✓	×	×
[139], [140]	✓	✓	✓	✓	✓
[138]	✓	✓	✓	×	×

structure of these configurations, reverberating reflections arise between the walls and the breast skin.

To reduce the reflections found in the enclosed arrays configurations, an immersion medium, typically a gel is usually used to fill the array. This immersion medium, however, might attenuate the received signal from the breast under investigation. In addition, the position of the breast with respect to the array wall might be difficult to estimate with the presence of this medium. As for the accuracy, this type of configuration might be affected by the different breast sizes, and hence different distance separating the antennas from the breast. Flexible wearable antennas, proposed in the latest research [139], [140], can solve the different drawbacks seen in the configurations provided. For instance, they can be fixed on the breast with no immersion medium. As such, the distance separating the antennas and the breast is reduced. The need to scan the optimized position of the antennas is no longer required since the antennas are placed on the breast at different positions using multistatic measurements, which reduces the error associated with antenna position. In addition, the discomfort that could arise with the scanned patient from the gel is eliminated. To further enhance the flexibility and simplicity of this system, the antenna arrays can be located on a bra rather than the breast skin, which can also result ease the imaging process for the patient.

In their turn, these flexible antennas require to be fabricated from biocompatible material. They also need to have high bandwidth, in addition to a light weight to avoid any distress. The bra itself can have some limitations related to the breast size, and the total number of antennas that can be placed on it. For this, special care should be also placed on the design of the antennas.

Concerning the antennas, it is seen that the performance of the microwave breast imaging system is highly affected by the design of the antenna element and its structure. In fact, a superior performance in terms of image quality is realized with the arrays of larger number of antennas, with an optimized antenna design. For this, a suitable antenna for such arrays is required to have a small size, wide impedance BW, high efficiency to couple the needed power to the breast, and must be simple to fabricate, cost effective, and biocompatible.

As a conclusion, for a simplified design, with the flexibility to add more antennas if needed, while accepting possible antenna scanning for the optimized location, planar arrays can be used. If the optimized array configuration and antenna design are found, with no need to add more antennas, flexible antennas that can be placed on a bra are best to be used. This can avoid the discomfort of the immersion gel, the bulkiness of the hemispherical and enclosed fixed arrays, and the high cost of fabrication. Further improvements can be made to the design in [139], [140] by designing a flexible bra for different breast sizes, or several bras for different sizes. In addition, the performance could be further enhanced if more antennas are added. For this, a miniaturized antenna size is needed to fit large number of antennas on the breast surface.

VII. CONCLUSION

Microwave imaging is taking an important interest as a non-invasive, highly sensitive, and a safer diagnostic technique, with a low cost and low illumination power levels. It is highly promising for breast imaging for cancer detection, not requiring ionizing radiation nor breast compression. The antenna system contained in this technology functions as the main block responsible for transmitting and receiving the reflections from the breast, needed for image reconstruction. This paper serves as a comprehensive survey of antennas proposed for microwave imaging. The different antenna array configurations, in addition to the different antenna elements designs and enhancements, presented in the literature for breast imaging, have been investigated. An evaluation of all of the investigated designs has been then presented with concluding remarks. It was found that the antipodal Vivaldi antenna (AVA) and the monopole antennas, with slots or slits in their ground plane, are promising as antenna elements to be used in an array of antennas placed in a hemispherical configuration. Further improvements to the optimized array designs of the literature can be made by designing flexible bras for different breast sizes, where miniaturized antennas can be used to fit a large number of antennas on the bra, and hence further enhance the performance and patient experience.

REFERENCES

[1] N. Howlader, A. M. Noone, M. Krapcho, D. Miller, K. Bishop, S. F. Altekruse, C. L. Kosary, M. Yu, J. Ruhl, Z. Tatalovich, A. Mariotto, D. R. Lewis, H. S. Chen, E. J. Feuer, and K. A. Cronin, Eds. *SEER Cancer Statistics Review, 1975–2013*. Bethesda, MD, USA: National Cancer Institute, Apr. 2016. [Online]. Available: https://seer.cancer.gov/archive/csr/1975_2013/

[2] R. Siegel, D. Naishadham, and A. Jemal, "Cancer statistics, 2013," *CA, A Cancer J. Clinicians*, vol. 63, no. 1, pp. 11–30, Jan. 2013.

[3] C. Li, *Breast Cancer Epidemiology*. New York, NY, USA: Springer, 2010.

[4] D. Wörtge, J. Moll, V. Krozer, B. Bazrafshan, F. Hübner, C. Park, and T. Vogl, "Comparison of X-ray-Mammography and planar UWB microwave imaging of the breast: First results from a patient study," *Diagnostics*, vol. 8, no. 3, p. 54, Aug. 2018.

[5] S. Nass, I. Henderson, and J. Lashof, "Mammography and beyond: Developing technologies for the early detection of breast cancer," Nat. Cancer Policy Board, Inst. Med., Commission Life Stud, Nat. Res. Council, Washington, DC, USA, 2001.

[6] P. T. Huynh, A. M. Jarolimek, and S. Daye, "The false-negative mammogram.," *RadioGraphics*, vol. 18, no. 5, pp. 1137–1154, Sep. 1998.

[7] P. J. Kornguth, F. J. Keefe, K. R. Wright, and D. M. Delong, "Mammography pain in women treated conservatively for breast cancer," *J. Pain*, vol. 1, no. 4, pp. 268–274, Jan. 2000.

[8] N. Nikolova, "Microwave imaging for breast cancer," *IEEE Microw. Mag.*, vol. 12, no. 7, pp. 78–94, Dec. 2011.

[9] L. L. Humphrey, M. Helfand, B. K. Chan, and S. H. Woolf, "Breast cancer screening: A summary of the evidence for the US preventive services task force," *Ann. Internal Med.*, vol. 137, no. 5, pp. 347–360, 2002.

[10] R. D. Rosenberg, W. C. Hunt, M. R. Williamson, F. D. Gilliland, P. W. Wiest, C. A. Kelsey, C. R. Key, and M. N. Linver, "Effects of age, breast density, ethnicity, and estrogen replacement therapy on screening mammographic sensitivity and cancer stage at diagnosis: Review of 183,134 screening mammograms in Albuquerque, new Mexico," *Radiology*, vol. 209, no. 2, pp. 511–518, Nov. 1998.

[11] V. P. Jackson, R. E. Hendrick, S. A. Feig, and D. B. Kopans, "Imaging of the radiographically dense breast.," *Radiology*, vol. 188, no. 2, pp. 297–301, Aug. 1993.

[12] S. Kwon and S. Lee, "Recent advances in microwave imaging for breast cancer detection," *Int. J. Biomed. Imag.*, vol. 2016, pp. 1–26, Dec. 2016.

[13] M. A. Stuchly and E. C. Fear, "Microwave detection of breast cancer," *IEEE Trans. Microw. Theory Techn.*, vol. 48, no. 11, pp. 1854–1863, Nov. 2000.

[14] W. T. Joines, Y. Zhang, C. Li, and R. L. Jirtle, "The measured electrical properties of normal and malignant human tissues from 50 to 900 MHz," *Med. Phys.*, vol. 21, no. 4, pp. 547–550, Apr. 1994.

[15] E. C. Fear, S. C. Hagness, P. M. Meaney, M. Okoniewski, and M. A. Stuchly, "Enhancing breast tumor detection with near-field imaging," *IEEE Microw. Mag.*, vol. 3, no. 1, pp. 48–56, Mar. 2002.

[16] V. De Santis, J. M. Sill, J. Bourqui, and E. C. Fear, "Safety assessment of ultra-wideband antennas for microwave breast imaging," *Bioelectromagnetics*, vol. 33, no. 3, pp. 215–225, 2012.

[17] D. O'Loughlin, M. O'Halloran, B. M. Moloney, M. Glavin, E. Jones, and M. A. Elahi, "Microwave breast imaging: Clinical advances and remaining challenges," *IEEE Trans. Biomed. Eng.*, vol. 65, no. 11, pp. 2580–2590, Nov. 2018.

[18] R. Chandra, H. Zhou, I. Balasingham, and R. M. Narayanan, "On the opportunities and challenges in microwave medical sensing and imaging," *IEEE Trans. Biomed. Eng.*, vol. 62, no. 7, pp. 1667–1682, Jul. 2015.

[19] J. C. Bolomey, C. Pichot, and G. Garboriaud, "Planar microwave imaging camera for biomedical applications: Critical and prospective analysis of reconstruction algorithms," *Radio Sci.*, vol. 26, no. 2, pp. 541–549, Mar. 1991.

[20] L. Jofre, M. S. Hawley, A. Broquetas, E. de los Reyes, M. Ferrando, and A. R. Elias-Fuste, "Medical imaging with a microwave tomographic scanner," *IEEE Trans. Biomed. Eng.*, vol. 37, no. 3, pp. 303–312, Mar. 1990.

[21] E. C. Fear, "Microwave imaging of the breast," *Technol. Cancer Res. Treat.*, vol. 4, no. 1, pp. 69–82, 2005.

[22] E. C. Fear, P. M. Meaney, and M. A. Stuchly, "Microwaves for breast cancer detection?" *IEEE Potentials*, vol. 22, no. 1, pp. 12–18, Feb. 2003.

[23] M. Elahi, D. O'Loughlin, B. Lavoie, M. Glavin, E. Jones, E. Fear, and M. O'Halloran, "Evaluation of image reconstruction algorithms for confocal microwave imaging: Application to patient data," *Sensors*, vol. 18, no. 6, p. 1678, May 2018.

[24] S. C. Hagness, A. Taflove, and J. E. Bridges, "Two-dimensional FDTD analysis of a pulsed microwave confocal system for breast cancer detection: Fixed-focus and antenna-array sensors," *IEEE Trans. Biomed. Eng.*, vol. 45, no. 12, pp. 1470–1479, Dec. 1998.

[25] H. B. Lim, N. T. T. Nhung, E.-P. Li, and N. D. Thang, "Confocal microwave imaging for breast cancer detection: Delay-Multiply-and-Sum image reconstruction algorithm," *IEEE Trans. Biomed. Eng.*, vol. 55, no. 6, pp. 1697–1704, Jun. 2008.

[26] M. Klemm, I. J. Craddock, J. A. Leendertz, A. Preece, and R. Benjamin, "Improved delay-and-sum beamforming algorithm for breast cancer detection," *Int. J. Antennas Propag.*, vol. 2008, pp. 1–9, Jun. 2008.

[27] M. Klemm, J. A. Leendertz, D. Gibbins, I. J. Craddock, A. Preece, and R. Benjamin, "Microwave radar-based breast cancer detection: Imaging in inhomogeneous breast phantoms," *IEEE Antennas Wireless Propag. Lett.*, vol. 8, pp. 1349–1352, 2009.

[28] M. O'Halloran, M. Glavin, and E. Jones, "Improved confocal microwave imaging of the breast using path-dependent signal weighting," in *Proc. 30th URSI Gen. Assem. Sci. Symp.*, Aug. 2011, pp. 1–4.

[29] Y. Xie, B. Guo, L. Xu, J. Li, and P. Stoica, "Multistatic adaptive microwave imaging for early breast cancer detection," *IEEE Trans. Biomed. Eng.*, vol. 53, no. 8, pp. 1647–1657, Aug. 2006.

[30] S. Y. Semenov, R. H. Svenson, A. E. Boulyshev, A. E. Souvorov, V. Y. Borisov, Y. Sizov, A. N. Starostin, K. R. Dezern, G. P. Tatsis, and V. Y. Baranov, "Microwave tomography: Two-dimensional system for biological imaging," *IEEE Trans. Biomed. Eng.*, vol. 43, no. 9, pp. 869–877, Sep. 1996.

[31] K. D. Paulsen, S. P. Poplack, D. Li, M. W. Fanning, and P. M. Meaney, "A clinical prototype for active microwave imaging of the breast," *IEEE Trans. Microw. Theory Techn.*, vol. 48, no. 11, pp. 1841–1853, Nov. 2000.

[32] A. E. Souvorov, A. E. Bulyshev, S. Y. Semenov, R. H. Svenson, and G. P. Tatsis, "Two-dimensional computer analysis of a microwave flat antenna array for breast cancer tomography," *IEEE Trans. Microw. Theory Techn.*, vol. 48, no. 8, pp. 1413–1415, Aug. 2000.

[33] I. Catapano, L. Di Donato, L. Crocco, O. M. Bucci, A. F. Morabito, T. Isernia, and R. Massa, "On quantitative microwave tomography of female breast," *Prog. Electromagn. Res.*, vol. 97, no. 9, pp. 75–93, 2009.

[34] T. M. Grzegorczyk, P. M. Meaney, P. A. Kaufman, R. M. di Florio-Alexander, and K. D. Paulsen, "Fast 3-D tomographic microwave imaging for breast cancer detection," *IEEE Trans. Med. Imag.*, vol. 31, no. 8, pp. 1584–1592, Aug. 2012.

[35] E. J. Bond, X. Li, S. C. Hagness, and B. D. Van Veen, "Microwave imaging via space-time beamforming for early detection of breast cancer," *IEEE Trans. Antennas Propag.*, vol. 51, no. 8, pp. 1690–1705, Aug. 2003.

[36] X. Li, S. K. Davis, S. C. Hagness, D. W. vanderWeide, and B. D. Vanveen, "Microwave imaging via space–time beamforming: Experimental investigation of tumor detection in multilayer breast phantoms," *IEEE Trans. Microw. Theory Techn.*, vol. 52, no. 8, pp. 1856–1865, Aug. 2004.

[37] X. Li, E. J. Bond, B. D. Van Veen, and S. C. Hagness, "An overview of ultra-wideband microwave imaging via space-time beamforming for early-stage breast-cancer detection," *IEEE Antennas Propag. Mag.*, vol. 47, no. 1, pp. 19–34, Feb. 2005.

[38] E. C. Fear, J. Bourqui, C. Curtis, D. Mew, B. Docktor, and C. Romano, "Microwave breast imaging with a monostatic radar-based system: A study of application to patients," *IEEE Trans. Microw. Theory Techn.*, vol. 61, no. 5, pp. 2119–2128, May 2013.

[39] S. Kwon and S. Lee, "Instantaneous microwave imaging with time-domain measurements for breast cancer detection," *Electron. Lett.*, vol. 49, no. 10, pp. 639–641, May 2013.

[40] S. Latif, D. Flores-Tapia, S. Pistorius, and L. Shafai, "A planar ultrawideband elliptical monopole antenna with reflector for breast microwave imaging," *Microw. Opt. Technol. Lett.*, vol. 56, no. 4, pp. 808–813, Apr. 2014.

[41] E. A. Cheever and K. R. Foster, "Microwave radiometry in living tissue: What does it measure?" *IEEE Trans. Biomed. Eng.*, vol. 39, no. 6, pp. 563–568, Jun. 1992.

[42] S. Jacobsen and P. R. Stauffer, "Nonparametric 1-D temperature restoration in lossy media using Tikhonov regularization on sparse radiometry data," *IEEE Trans. Biomed. Eng.*, vol. 50, no. 2, pp. 178–188, Feb. 2003.

[43] B. Bocquet, J. C. van de Velde, A. Mamouni, Y. Leroy, G. Giaux, J. Delannoy, and D. Delvalee, "Microwave radiometric imaging at 3 GHz for the exploration of breast tumors," *IEEE Trans. Microw. Theory Techn.*, vol. 38, no. 6, pp. 791–793, Jun. 1990.

[44] R. A. Kruger, K. K. Kopecky, A. M. Aisen, D. R. Reinecke, G. A. Kruger, and W. L. Kiser, "Thermoacoustic CT with radio waves: A medical imaging paradigm," *Radiology*, vol. 211, no. 1, pp. 275–278, Apr. 1999.

[45] "Revision of part 15 of the commission's rules regarding ultra-wideband transmission systems," Tech. Rep. FCC 02-48, Federal Commun. Commission, Washington, DC, USA, 2002.
[46] M. Fernando, K. Busawon, M. Elsdon, and D. Smith, "Fundamental issues in antenna design for microwave medical imaging applications," in *Proc. 7th Int. Symp. Commun. Syst., Netw. Digit. Signal Process. (CSNDSP)*, Jul. 2010, pp. 795–800.
[47] R. C. Conceição, J. J. Mohr, and M. O'Halloran, *An Introduction to Microwave Imaging for Breast Cancer Detection*. Basel, Switzerland: Springer, 2016.
[48] *IEEE Standard for Safety Levels With Respect to Human Exposure to Radio Frequency Electromagnetic Fields 3 kHz to 300 GHz*, Institute of Electrical and Electronics Engineers (IEEE) Standard C95.1-1999, 1999.
[49] *IEEE Recommended Practice for Measurements and Computations of Radio Frequency Electromagnetic Fields With Respect to Human Exposure to Such Fields, 100 kHz-300 GHz*, IEEE Standards Association C95.3-2002, 2002.
[50] N. Joachimowicz, C. Conessa, T. Henriksson, and B. Duchêne, "Breast phantoms for microwave imaging," *IEEE Antennas Wireless Propag. Lett.*, vol. 13, pp. 1333–1336, 2014.
[51] N. Joachimowicz, B. Duchêne, C. Conessa, and O. Meyer, "Easy-to-produce adjustable realistic breast phantoms for microwave imaging," in *Proc. 10th Eur. Conf. Antennas Propag. (EuCAP)*, Apr. 2016, pp. 1–4.
[52] Y. Baskharoun, A. Trehan, N. K. Nikolova, and M. D. Noseworthy, "Physical phantoms for microwave imaging of the breast," in *Proc. IEEE Topical Conf. Biomed. Wireless Technol., Netw., Sens. Syst. (BioWireleSS)*, Jan. 2012, pp. 73–76.
[53] S. Chaudhary, R. Mishra, A. Swarup, and J. M. Thomas, "Dielectric properties of normal & malignant human breast tissues at radiowave & microwave frequencies," *Indian J. Biochem. Biophys.*, vol. 21, no. 1, pp. 76–79, Feb. 1984.
[54] A. Campbell and D. Land, "Dielectric properties of female human breast tissue measured *in vitro* at 3.2 GHz," *Phys. Med. Biol.*, vol. 37, no. 1, p. 193, 1992.
[55] M. Lazebnik, D. Popovic, L. McCartney, C. B. Watkins, M. J. Lindstrom, J. Harter, S. Sewall, T. Ogilvie, A. Magliocco, T. M. Breslin, W. Temple, D. Mew, J. H. Booske, M. Okoniewski, and S. C. Hagness, "A large-scale study of the ultrawideband microwave dielectric properties of normal, benign and malignant breast tissues obtained from cancer surgeries," *Phys. Med. Bio.*, vol. 52, no. 20, p. 6093, Oct. 2007.
[56] X. Li and S. C. Hagness, "A confocal microwave imaging algorithm for breast cancer detection," *IEEE Microw. Wireless Compon. Lett.*, vol. 11, no. 3, pp. 130–132, Mar. 2001.
[57] J. M. Sill and E. C. Fear, "Tissue sensing adaptive radar for breast cancer detection—Experimental investigation of simple tumor models," *IEEE Trans. Microw. theory Techn.*, vol. 53, no. 11, pp. 3312–3319, Nov. 2005.
[58] M. Chiappe and G. L. Gragnani, "Vivaldi antennas for microwave imaging: Theoretical analysis and design considerations," *IEEE Trans. Instrum. Meas.*, vol. 55, no. 6, pp. 1885–1891, Dec. 2006.
[59] R. Janaswamy and D. Schaubert, "Analysis of the tapered slot antenna," *IEEE Trans. Antennas Propag.*, vol. 35, no. 9, pp. 1058–1065, Sep. 1987.
[60] Z. Wang and H. Zhang, "Improvements in a high gain UWB antenna with corrugated edges," *Prog. Electromagn. Res. C*, vol. 6, pp. 159–166, 2009.
[61] M. Abbak, M. N. Akıncı, M. Çayören, and I. Akduman, "Experimental microwave imaging with a novel corrugated Vivaldi antenna," *IEEE Trans. Antennas Propag.*, vol. 65, no. 6, pp. 3302–3307, Jun. 2017.
[62] G. K. Pandey and M. K. Meshram, "A printed high gain UWB vivaldi antenna design using tapered corrugation and grating elements," *Int. J. RF Microw. Comput.-Aided Eng.*, vol. 25, no. 7, pp. 610–618, Sep. 2015.
[63] J. Bourqui, M. Okoniewski, and E. C. Fear, "Balanced antipodal vivaldi antenna with dielectric director for near-field microwave imaging," *IEEE Trans. Antennas Propag.*, vol. 58, no. 7, pp. 2318–2326, Jul. 2010.
[64] J. Bourqui, M. A. Campbell, T. Williams, and E. C. Fear, "Antenna evaluation for ultra-wideband microwave imaging," *Int. J. Antennas Propag.*, vol. 2010, pp. 1–8, May 2010.
[65] S. Nikolaou, G. E. Ponchak, J. Papapolymerou, and M. M. Tentzeris, "Conformal double exponentially tapered slot antenna (DETSA) on LCP for UWB applications," *IEEE Trans. Antennas Propag.*, vol. 54, no. 6, pp. 1663–1669, Jun. 2006.
[66] M. C. Greenberg, K. L. Virga, and C. L. Hammond, "Performance characteristics of the dual exponentially tapered slot antenna (DETSA) for wireless communications applications," *IEEE Trans. Veh. Technol.*, vol. 52, no. 2, pp. 305–312, Mar. 2003.
[67] C. Deng and Y.-j. Xie, "Design of resistive loading Vivaldi antenna," *IEEE Antennas Wireless Propag. Lett.*, vol. 8, pp. 240–243, 2009.
[68] J. Bai, S. Shi, and D. W. Prather, "Modified compact antipodal Vivaldi antenna for 4–50-GHz UWB application," *IEEE Trans. Microw. Theory Techn.*, vol. 59, no. 4, pp. 1051–1057, Apr. 2011.
[69] B. Biswas, R. Ghatak, and D. R. Poddar, "A fern fractal leaf inspired wideband antipodal Vivaldi antenna for microwave imaging system," *IEEE Trans. Antennas Propag.*, vol. 65, no. 11, pp. 6126–6129, Nov. 2017.
[70] M. J. Ammann and Z. N. Chen, "Wideband monopole antennas for multi-band wireless systems," *IEEE Antennas Propag. Mag.*, vol. 45, no. 2, pp. 146–150, Apr. 2003.
[71] N. P. Agrawall, G. Kumar, and K. P. Ray, "Wide-band planar monopole antennas," *IEEE Trans. Antennas Propag.*, vol. 46, no. 2, pp. 294–295, Feb. 1998.
[72] M. Ahadi, W. Z. W. Hasan, M. I. B. Saripan, and M. B. M. Isa, "Square monopole antenna for microwave imaging, design and characterisation," *IET Microw., Antennas Propag.*, vol. 9, no. 1, pp. 49–57, Jan. 2015.
[73] K. Halili, M. Ojaroudi, and N. Ojaroudi, "Ultrawideband monopole antenna for use in a circular cylindrical microwave imaging system," *Microw. Opt. Technol. Lett.*, vol. 54, no. 9, pp. 2202–2205, Sep. 2012.
[74] M. Ojaroudi, C. Ghobadi, and J. Nourinia, "Small square monopole antenna with inverted T-Shaped notch in the ground plane for UWB application," *IEEE Antennas Wireless Propag. Lett.*, vol. 8, pp. 728–731, 2009.
[75] A. Abdollahvand, A. Pirhadi, H. Ebrahimian, and M. Abdollahvand, "A compact UWB printed antenna with bandwidth enhancement for in-body microwave imaging applications," *Prog. Electromagn. Res. C*, vol. 55, no. 10, pp. 149–157, 2014.
[76] N. Ojaroudi and N. Ghadimi, "Omnidirectional microstrip monopole antenna design for use in microwave imaging systems," *Microw. Opt. Technol. Lett.*, vol. 57, no. 2, pp. 395–401, Feb. 2015.
[77] N. Ojaroudi, M. Ojaroudi, and Y. Ebazadeh, "UWB/omni-directional microstrip monopole antenna for microwave imaging applications," *Prog. Electromagn. Res. C*, vol. 47, no. 2, pp. 139–146, 2014.
[78] M. H. Bah, J. Hong, and D. A. Jamro, "Ground slotted monopole antenna design for microwave breast cancer detection based on time reversal music," *Prog. Electromagn. Res. C*, vol. 59, no. 4, pp. 117–126, 2015.
[79] N. Ojaroudi, M. Ojaroudi, and N. Ghadimi, "UWB omnidirectional square monopole antenna for use in circular cylindrical microwave imaging systems," *IEEE Antennas Wireless Propag. Lett.*, vol. 11, pp. 1350–1353, 2012.
[80] M. Ojaroudi and O. A. Civi, "High efficiency loop sleeve monopole antenna for array based UWB microwave imaging systems," in *Proc. IEEE Int. Symp. Antennas Propag. (APSURSI)*, Jun. 2016, pp. 1781–1782.
[81] W.-C. Liu and P.-C. Kao, "CPW-fed triangular monopole antenna for ultra-wideband operation," *Microw. Opt. Technol. Lett.*, vol. 47, no. 6, pp. 580–582, 2005.
[82] A. Eesuola, Y. Chen, and G. Y. Tian, "Novel ultra-wideband directional antennas for microwave breast cancer detection," in *Proc. IEEE Int. Symp. Antennas Propag. (APSURSI)*, Jul. 2011, pp. 90–93.
[83] S. Mondal and P. P. Sarkar, "A novel design of compact wideband hexagonal antenna," *Microw. Opt. Technol. Lett.*, vol. 55, no. 1, pp. 1–4, Jan. 2013.
[84] H. M. Jafari, M. J. Deen, S. Hranilovic, and N. K. Nikolova, "A study of ultrawideband antennas for near-field imaging," *IEEE Trans. Antennas Propag.*, vol. 55, no. 4, pp. 1184–1188, Apr. 2007.
[85] S. Subramanian, B. Sundarambal, and D. Nirmal, "Investigation on simulation-based specific absorption rate in ultra-wideband antenna for breast cancer detection," *IEEE Sensors J.*, vol. 18, no. 24, pp. 10002–10009, Dec. 2018.
[86] M. Jalilvand, C. Vasanelli, C. Wu, J. Kowalewski, and T. Zwick, "On the evaluation of a proposed bowtie antenna for microwave tomography," in *Proc. 8th Eur. Conf. Antennas Propag. (EuCAP)*, Apr. 2014, pp. 2790–2794.
[87] J.-Y. Sze and K.-L. Wong, "Bandwidth enhancement of a microstrip-line-fed printed wide-slot antenna," *IEEE Trans. Antennas Propag.*, vol. 49, no. 7, pp. 1020–1024, Jul. 2001.
[88] D. Gibbins, M. Klemm, I. J. Craddock, J. A. Leendertz, A. Preece, and R. Benjamin, "A comparison of a wide-slot and a stacked patch antenna for the purpose of breast cancer detection," *IEEE Trans. Antennas Propag.*, vol. 58, no. 3, pp. 665–674, Mar. 2010.

[89] Y. Wang, A. E. Fathy, and M. R. Mahfouz, "Novel compact tapered microstrip slot antenna for microwave breast imaging," in *Proc. IEEE Int. Symp. Antennas Propag. (APSURSI)*, Jul. 2011, pp. 2119–2122.

[90] H. Kanj and M. Popovic, "Miniaturized microstrip-fed' Dark Eyes' antenna for near-field microwave sensing," *IEEE Antennas Wireless Propag. Lett.*, vol. 4, pp. 397–401, 2005.

[91] H. Kanj and M. Popovic, "A novel ultra-compact broadband antenna for microwave breast tumor detection," *Prog. Electromagn. Res.*, vol. 86, no. 9, pp. 169–198, 2008.

[92] D. A. Woten and M. El-Shenawee, "Broadband dual linear polarized antenna for statistical detection of breast cancer," *IEEE Trans. Antennas Propag.*, vol. 56, no. 11, pp. 3576–3580, Nov. 2008.

[93] M. Z. Mahmud, M. T. Islam, and M. Samsuzzaman, "A high performance UWB antenna design for microwave imaging system," *Microw. Opt. Technol. Lett.*, vol. 58, no. 8, pp. 1824–1831, Aug. 2016.

[94] C. A. Balanis, *Antenna Theory: Analysis and Design*. Hoboken, NJ, USA: Wiley, 2016.

[95] M. Solis Nepote, D. R. Herrera, D. F. Tapia, S. Latif, and S. Pistorius, "A comparison study between horn and vivaldi antennas for 1.5–6 GHz breast microwave radar imaging," in *Proc. 8th Eur. Conf. Antennas Propag. (EuCAP)*, Apr. 2014, pp. 59–62.

[96] X. Li, S. C. Hagness, M. K. Choi, and D. W. van der Weide, "Numerical and experimental investigation of an ultrawideband ridged pyramidal horn antenna with curved launching plane for pulse radiation," *IEEE Antennas Wireless Propag. Lett.*, vol. 2, pp. 259–262, 2003.

[97] A. M. Abbosh, H. K. Kan, and M. E. Bialkowski, "Design of compact directive ultra wideband antipodal antenna," *Microw. Opt. Technol. Lett.*, vol. 48, no. 12, pp. 2448–2450, 2006.

[98] A. M. Abbosh, "Directive antenna for ultrawideband medical imaging systems," *Int. J. Antennas Propag.*, vol. 2008, Mar. 2008, Art. no. 854012.

[99] A. M. Abbosh, H. K. Kan, and M. E. Bialkowski, "Compact ultra-wideband planar tapered slot antenna for use in a microwave imaging system," *Microw. Opt. Technol. Lett.*, vol. 48, no. 11, pp. 2212–2216, 2006.

[100] A. M. Abbosh, "Miniaturized microstrip-fed tapered-slot antenna with ultrawideband performance," *IEEE Antennas Wireless Propag. Lett.*, vol. 8, pp. 690–692, 2009.

[101] B. J. Mohammed, A. M. Abbosh, and M. E. Bialkowski, "Design of tapered slot antenna operating in coupling liquid for ultrawideband microwave imaging systems," in *Proc. IEEE Int. Symp. Antennas Propag. (APSURSI)*, Jul. 2011, pp. 145–148.

[102] A. Molaei, A. G. Dagheyan, J. H. Juesas, and J. Martinez-Lorenzo, "Miniaturized UWB antipodal vivaldi antenna for a mechatronic breast cancer imaging system," in *Proc. IEEE Int. Symp. Antennas Propag. USNC/URSI Nat. Radio Sci. Meeting*, Jul. 2015, pp. 352–353.

[103] X. Yun, E. C. Fear, and R. H. Johnston, "Compact antenna for radar-based breast cancer detection," *IEEE Trans. Antennas Propag.*, vol. 53, no. 8, pp. 2374–2380, Aug. 2005.

[104] X. Li, M. Jalilvand, Y. L. Sit, and T. Zwick, "A compact double-layer on-body matched bowtie antenna for medical diagnosis," *IEEE Trans. Antennas Propag.*, vol. 62, no. 4, pp. 1808–1816, Apr. 2014.

[105] M. T. Islam, M. Z. Mahmud, N. Misran, J.-I. Takada, and M. Cho, "Microwave breast phantom measurement system with compact side slotted directional antenna," *IEEE Access*, vol. 5, pp. 5321–5330, 2017.

[106] S. Guruswamy, R. Chinniah, and K. Thangavelu, "A printed compact UWB Vivaldi antenna with Hemi cylindrical slots and directors for microwave imaging applications," *AEU-Int. J. Electron. Commun.*, vol. 110, Oct. 2019, Art. no. 152870.

[107] D.-M. In, M.-J. Lee, D. Kim, C.-Y. Oh, and Y.-S. Kim, "Antipodal linearly tapered slot antenna using unequal half-circular defected sides for gain improvements," *Microw. Opt. Technol. Lett.*, vol. 54, no. 8, pp. 1963–1965, Aug. 2012.

[108] M. Moosazadeh and S. Kharkovsky, "A compact high-gain and Front-to-Back ratio elliptically tapered antipodal vivaldi antenna with trapezoid-shaped dielectric lens," *IEEE Antennas Wireless Propag. Lett.*, vol. 15, pp. 552–555, 2016.

[109] M. Moosazadeh, S. Kharkovsky, J. T. Case, and B. Samali, "Improved radiation characteristics of small antipodal Vivaldi antenna for microwave and millimeter-wave imaging applications," *IEEE Antennas Wireless Propag. Lett.*, vol. 16, pp. 1961–1964, 2017.

[110] G. Teni, N. Zhang, J. Qiu, and P. Zhang, "Research on a novel miniaturized antipodal Vivaldi antenna with improved radiation," *IEEE Antennas Wireless Propag. Lett.*, vol. 12, pp. 417–420, 2013.

[111] A. M. De Oliveira, M. B. Perotoni, S. T. Kofuji, and J. F. Justo, "A palm tree antipodal Vivaldi antenna with exponential slot edge for improved radiation pattern," *IEEE Antennas Wireless Propag. Lett.*, vol. 14, pp. 1334–1337, 2015.

[112] L. Juan, F. Guang, Y. Lin, and F. Demin, "A modified balanced antipodal Vivaldi antenna with improved radiation characteristics," *Microw. Opt. Technol. Lett.*, vol. 55, no. 6, pp. 1321–1325, Jun. 2013.

[113] P. Fei, Y.-C. Jiao, W. Hu, and F.-S. Zhang, "A miniaturized antipodal Vivaldi antenna with improved radiation characteristics," *IEEE Antennas Wireless Propag. Lett.*, vol. 10, pp. 127–130, 2011.

[114] A. Molaei, M. Kaboli, M. S. Abrishamian, and S. A. Mirtaheri, "Dielectric lens balanced antipodal Vivaldi antenna with low cross-polarisation for ultra-wideband applications," *IET Microw., Antennas Propag.*, vol. 8, no. 14, pp. 1137–1142, Nov. 2014.

[115] K. Kota and L. Shafai, "Gain and radiation pattern enhancement of balanced antipodal Vivaldi antenna," *Electron. Lett.*, vol. 47, no. 5, pp. 303–304, Mar. 2011.

[116] M. Abbak, M. Çayören, and I. Akduman, "Microwave breast phantom measurements with a cavity-backed vivaldi antenna," *IET Microw., Antennas Propag.*, vol. 8, no. 13, pp. 1127–1133, Oct. 2014.

[117] J. J. Golezani, M. Abbak, and I. Akduman, "Modified directional wide band printed monopole antenna for use in radar and microwave imaging applications," *Prog. Electromagn. Res. Lett.*, vol. 33, no. 6, pp. 119–129, 2012.

[118] A. A. Lestari, E. Bharata, A. B. Suksmono, A. Kurniawan, A. G. Yarovoy, and L. P. Ligthart, "A modified bow-tie antenna for improved pulse radiation," *IEEE Trans. Antennas Propag.*, vol. 58, no. 7, pp. 2184–2192, Jul. 2010.

[119] C. H. See, R. A. Abd-Alhameed, S. W. J. Chung, D. Zhou, H. Al-Ahmad, and P. S. Excell, "The design of a resistively loaded bowtie antenna for applications in breast cancer detection systems," *IEEE Trans. Antennas Propag.*, vol. 60, no. 5, pp. 2526–2530, May 2012.

[120] A. A. Lestari, A. G. Yarovoy, and L. P. Ligthart, "RC-loaded bow-tie antenna for improved pulse radiation," *IEEE Trans. Antennas Propag.*, vol. 52, no. 10, pp. 2555–2563, Oct. 2004.

[121] C. J. Shannon, E. C. Fear, and M. Okoniewski, "Dielectric-filled slotline bowtie antenna for breast cancer detection," *Electron. Lett.*, vol. 41, no. 7, pp. 388–390, Mar. 2005.

[122] R. Khalaj Amineh, A. Trehan, and N. K. Nikolova, "TEM horn antenna for ultra-wide band microwave breast imaging," *Prog. Electromagn. Res. B*, vol. 13, no. 3, pp. 59–74, 2009.

[123] R. K. Amineh, M. Ravan, A. Trehan, and N. K. Nikolova, "Near-field microwave imaging based on aperture raster scanning with TEM horn antennas," *IEEE Trans. Antennas Propag.*, vol. 59, no. 3, pp. 928–940, Mar. 2011.

[124] S. C. Hagness, A. Taflove, and J. E. Bridges, "Three-dimensional FDTD analysis of a pulsed microwave confocal system for breast cancer detection: Design of an antenna-array element," *IEEE Trans. Antennas Propag.*, vol. 47, no. 5, pp. 783–791, May 1999.

[125] K. Moussakhani, R. K. Amineh, and N. K. Nikolova, "High-efficiency TEM horn antenna for ultra-wide band microwave tissue imaging," in *Proc. IEEE Int. Symp. Antennas Propag. (APSURSI)*, Jul. 2011, pp. 127–130.

[126] M. A. Hernández-López, M. Quintillán-González, S. González García, A. R. Bretones, and R. G. Martín, "A rotating array of antennas for confocal microwave breast imaging," *Microw. Opt. Technol. Lett.*, vol. 39, no. 4, pp. 307–311, Nov. 2003.

[127] H. M. Jafari, J. M. Deen, S. Hranilovic, and N. K. Nikolova, "Co-polarised and cross-polarised antenna arrays for breast, cancer detection," *IET Microw., Antennas Propag.*, vol. 1, no. 5, pp. 1055–1058, Oct. 2007.

[128] T. Sugitani, S. Kubota, A. Toya, X. Xiao, and T. Kikkawa, "A compact 4x4 planar UWB antenna array for 3-D breast cancer detection," *IEEE Antennas Wireless Propag. Lett.*, vol. 12, pp. 733–736, 2013.

[129] M. Bassi, M. Caruso, M. S. Khan, A. Bevilacqua, A.-D. Capobianco, and A. Neviani, "An integrated microwave imaging radar with planar antennas for breast cancer detection," *IEEE Trans. Microw. Theory Techn.*, vol. 61, no. 5, pp. 2108–2118, May 2013.

[130] M. J. Burfeindt, N. Behdad, B. D. Van Veen, and S. C. Hagness, "Quantitative microwave imaging of realistic numerical breast phantoms using an enclosed array of multiband, miniaturized patch antennas," *IEEE Antennas Wireless Propag. Lett.*, vol. 11, pp. 1626–1629, 2012.

[131] S. M. Aguilar, M. A. Al-Joumayly, M. J. Burfeindt, N. Behdad, and S. C. Hagness, "Multiband miniaturized patch antennas for a compact, shielded microwave breast imaging array," *IEEE Trans. Antennas Propag.*, vol. 62, no. 3, pp. 1221–1231, Mar. 2014.
[132] P. Mojabi and J. LoVetri, "A novel microwave tomography system using a rotatable conductive enclosure," *IEEE Trans. Antennas Propag.*, vol. 59, no. 5, pp. 1597–1605, May 2011.
[133] M. Haynes, J. Stang, and M. Moghaddam, "Microwave breast imaging system prototype with integrated numerical characterization," *Int. J. Biomed. Imag.*, vol. 2012, pp. 1–18, Mar. 2012.
[134] R. Nilavalan, I. J. Craddock, A. Preece, J. Leendertz, and R. Benjamin, "Wideband microstrip patch antenna design for breast cancer tumour detection," *IET Microw., Antennas Propag.*, vol. 1, no. 2, pp. 277–281, Apr. 2007.
[135] M. Klemm, I. J. Craddock, J. A. Leendertz, A. Preece, and R. Benjamin, "Radar-based breast cancer detection using a hemispherical antenna array—Experimental results," *IEEE Trans. Antennas Propag.*, vol. 57, no. 6, pp. 1692–1704, Jun. 2009.
[136] M. Klemm, J. A. Leendertz, D. Gibbins, I. J. Craddock, A. Preece, and R. Benjamin, "Microwave radar-based differential breast cancer imaging: Imaging in homogeneous breast phantoms and low contrast scenarios," *IEEE Trans. Antennas Propag.*, vol. 58, no. 7, pp. 2337–2344, Jul. 2010.
[137] M. Klemm, I. J. Craddock, A. Preece, J. Leendertz, and R. Benjamin, "Evaluation of a hemi-spherical wideband antenna array for breast cancer imaging," *Radio Sci.*, vol. 43, no. 6, pp. 1–15, Dec. 2008.
[138] M. Jalilvand, T. Zwick, L. Zwirello, and X. Li, "Ultra wideband compact near-field imaging system for breast cancer detection," *IET Microw., Antennas Propag.*, vol. 9, no. 10, pp. 1009–1014, Jul. 2015.
[139] H. Bahramiabarghouei, E. Porter, A. Santorelli, B. Gosselin, M. Popovic, and L. A. Rusch, "Flexible 16 antenna array for microwave breast cancer detection," *IEEE Trans. Biomed. Eng.*, vol. 62, no. 10, pp. 2516–2525, Oct. 2015.
[140] E. Porter, H. Bahrami, A. Santorelli, B. Gosselin, L. A. Rusch, and M. Popović, "A wearable microwave antenna array for time-domain breast tumor screening," *IEEE Trans. Med. Imag.*, vol. 35, no. 6, pp. 1501–1509, Jun. 2016.
[141] E. Porter, E. Kirshin, A. Santorelli, M. Coates, and M. Popović, "Time-domain multistatic radar system for microwave breast screening," *IEEE Antennas Wireless Propag. Lett.*, vol. 12, pp. 229–232, 2013.

HILAL M. EL MISILMANI (Member, IEEE) was born in Beirut, Lebanon, in 1987. He received the B.E. degree in communications and electronics engineering from Beirut Arab University, Lebanon, in 2010, and the M.E. and Ph.D. degrees in electrical and computer engineering from the American University of Beirut, Beirut, in 2012 and 2015 respectively.

From August 2011 to September 2012, he was a Telecommunications Engineer with Dar Al-Handasah Consultants (Shair and Partners). From September 2012 to August 2014, he was a Researcher with the Beirut Research and Innovation Center. From September 2014 to May 2015, he was a Lecturer with the American University of Beirut, where he was also a Research Associate, from June 2015 to September 2016. Since September 2015, he has been an Assistant Professor with the Electrical and Computer Engineering Department, Beirut Arab University. He is the author of more than 20 articles. His research interests include the design of high-power microwave antennas, slotted waveguide antennas and Vlasov antennas, the design and applications of antenna arrays, antennas for biomedical applications, and machine learning in antenna design.

Dr. El Misilmani was a recipient of several scholarships, the Rafic Hariri Foundation Scholarship, from September 2005 to June 2010, the Association of Specialization and Scientific Guidance (SSG) Scholarship, from February 2006 to June 2010, the Lebanese Association for Scientific Research (LASeR) Scholarship, from September 2013 to May 2015, and the National Council for Scientific Research (CNRS) Doctoral Scholarship Award, from 2013 to May 2015.

TAREK NAOUS (Student Member, IEEE) is currently pursuing the B.E. degree in communications and electronics engineering with Beirut Arab University (BAU). He is an Undergraduate Research Assistant with the Radio Frequency and Antenna Design Research Team, BAU. He has served as the IEEE Student Branch Chairperson at the Faculty of Engineering for two years. He has previously authored a survey article on the use of machine learning in antenna design and has several manuscripts under revision. His research interests include machine learning and machine learning in communications.

SALWA K. AL KHATIB (Student Member, IEEE) is currently pursuing the B.E. degree in computer engineering with Beirut Arab University (BAU). She is an Undergraduate Research Assistant with the Radio Frequency and Antenna Design Research Team, BAU. She has been serving as the IEEE Student Branch Chairperson at the Faculty of Engineering, since September 2019. Her research interests include machine learning and its general applications and intelligent transportation systems.

KARIM Y. KABALAN (Member, IEEE) was born in Jbeil, Lebanon. He received the B.S. degree in physics from Lebanese University, in 1979, and the M.S. and Ph.D. degrees in electrical and computer engineering from Syracuse University, in 1983 and 1985, respectively.

In 1986, he was a Visiting Assistant Professor of electrical and computer engineering with Syracuse University. He is currently a Professor of electrical and computer engineering with the Electrical and Computer Engineering Department, Faculty of Engineering and Architecture, American University of Beirut. He is the author of two copyrighted software, six book chapters, more than 100 journal articles, and more than 124 conference papers. His research interests include electromagnetic and radio frequency, microstrip antenna design by using sophisticated patch element and array theoretical modelling techniques, cognitive radio antenna, and MIMO antenna systems.